

UNCLASSIFIED

AD NUMBER
AD811299
NEW LIMITATION CHANGE
TO Approved for public release, distribution unlimited
FROM Distribution authorized to U.S. Gov't. agencies and their contractors; Administrative/Operational use; Jan 1967. Other requests shall be referred to Metals and Ceramics Division, AFML, RTD Wright-Patterson AFB, OH 45433.
AUTHORITY
USAFML ltr, 29 Mar 1972

THIS PAGE IS UNCLASSIFIED

811299

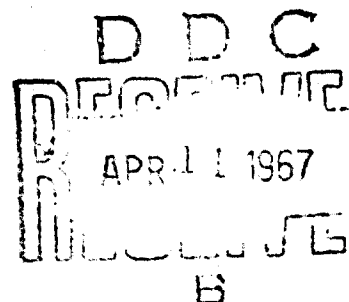
A FUNDAMENTAL INVESTIGATION OF THE NATURE OF STRESS-CORROSION CRACKING IN ALUMINUM ALLOYS

*F. H. HAYNIE, D. A. VAUGHAN, D. I. PHALEN,
W. K. BOYD, and P. D. FROST*

BATTELLE MEMORIAL INSTITUTE

TECHNICAL REPORT AFML-TR-66-267

JANUARY 1967



This document is subject to special export controls and each transmittal to foreign governments or foreign nationals may be made only with prior approval of the Metals and Ceramics Division (MAM), Air Force Materials Laboratory, Wright-Patterson Air Force Base, Ohio 45433.

**AIR FORCE MATERIALS LABORATORY
RESEARCH AND TECHNOLOGY DIVISION
AIR FORCE SYSTEMS COMMAND
WRIGHT-PATTERSON AIR FORCE BASE, OHIO**

**Reproduced From
Best Available Copy**

NOTICES

When Government drawings, specifications, or other data are used for any purpose other than in connection with a definitely related Government procurement operation, the United States Government thereby incurs no responsibility nor any obligation whatsoever; and the fact that the Government may have formulated, furnished, or in any way supplied the said drawings, specifications, or other data, is not to be regarded by implication or otherwise as in any manner licensing the holder or any other person or corporation, or conveying any rights or permission to manufacture, use, or sell any patented invention that may in any way be related thereto.

Copies of this report should not be returned to the Research and Technology Division unless return is required by security considerations, contractual obligations, or notice on a specific document.

A FUNDAMENTAL INVESTIGATION OF THE NATURE OF STRESS-CORROSION CRACKING IN ALUMINUM ALLOYS

*F. H. HAYNIE, D. A. VAUGHAN, D. I. PHALEN,
W. K. BOYD, and P. D. FROST*

This document is subject to special export controls and each transmittal to foreign governments or foreign nationals may be made only with prior approval of the Metals and Ceramics Division (MAM), Air Force Materials Laboratory, Wright-Patterson Air Force Base, Ohio 45433.

FOREWORD

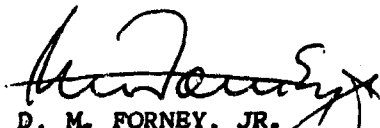
This report was prepared by Battelle Memorial Institute, Columbus, Ohio, under USAF Contract No. AF 33(615)-1710. The contract was initiated under Project No. 7351, "Metallic Materials", Task No. 735106, "Behavior of Metals". The work was administered under the direction of the Metals and Ceramics Division of the Air Force Materials Laboratory, Research and Technology Division, Air Force Systems Command, with Mr. A. W. Brisbane acting as Technical Manager.

Contributions to this research were made by other members of the Battelle staff. D. N. Williams supervised the casting and fabricating of the high-purity alloys. R. B. Price and R. A. Ewing conducted the autoradiographic work. W. A. Brill performed the microstress analysis.

This report covers the period from June, 1965 to May, 1966.

The manuscript of this report was released by the authors in June, 1966, for publication as a Technical Report.

This technical report has been reviewed and is approved.


D. M. FORNEY, JR.
Actg Chief, Strength & Dynamics Branch
Metals and Ceramics Division

ABSTRACT

A review of the existing theories for the mechanism of stress-corrosion cracking indicated that the electrochemical-mechanical theory was most consistent with existing data for stress-corrosion cracking in high-strength aluminum alloys. However, experimental crack-kinetics studies did not reveal fast fracture steps which would be associated with such a mechanism. The cracking rates were well within the limits predicted by an electrochemical mechanism.

A statistically designed experiment to study the effects of metallurgical variables on stress-corrosion cracking behavior of high-purity 7039- and 7079-type alloys has revealed several important facts. Stress-corrosion-cracking susceptibility is a function of the stress normal to the grain boundaries rather than a function of the applied stress on these materials in thin sheet and plate form. Compensation for this effect was necessary before the effects of other metallurgical variables could be determined. Chromium-alloy additions, silver additions, a more severe than normal solution heat treatment, overaging, and the combination of silver and overaging or the combination of chromium and the more severe solution heat treatment were all beneficial to the stress-corrosion cracking resistance of these alloys. Copper additions were detrimental.

The combined results of electrochemical, autoradiographic, electron-transmission, and electron-replica studies strengthen the belief that cathodically produced hydrogen dissolved in strained grain boundaries is essential for the initiation of stress-corrosion cracking in these alloys. Based on these results a mechanism is proposed. This proposed mechanism involves the absorption of cathodically produced hydrogen into tensile-strained, mechanically weak (alloy-depleted zones) grain boundaries. The hydrogen acts to reduce the activation energy for anodic dissolution of the metal and thus accelerates the localized corrosion at the grain boundaries perpendicular to applied tensile stresses.

TABLE OF CONTENTS

	<u>Page</u>
INTRODUCTION	1
SUMMARY	1
REVIEW OF THEORY	2
The Electrochemical Theory	2
The Mechanical Theory	3
The Electrochemical-Mechanical Theory	4
The Surface-Energy Theory	5
EXPERIMENTAL WORK	6
Metallurgical-Variable Studies	6
Casting and Fabrication of Alloys	8
Tensile Properties	8
Preparation of Specimens	9
Stress-Corrosion Testing Procedure	13
Results	14
-Crack-Kinetics Studies	20
Calibration	25
Results	27
Electrochemical Studies	35
Autoradiographic Studies to Detect Minute Amounts of Tritium Absorbed	
Because of Tensile Stress	37
Precipitate-Phase Studies	39
Fracture-Face-Morphology and Surface-Reaction Studies	42
Microstress Studies	53
DISCUSSION OF RESULTS	54
Metallurgical-Variable Studies	54
Crack-Kinetics Studies	55
Electrochemical Studies	56
Autoradiographic Studies	56
Precipitate-Phase Studies	56
Fracture-Face Morphology and Surface-Reaction Studies	57
Microstress Studies	57
Consistency of the Results of the Independent Studies	57
PROPOSED MECHANISM FOR THE INITIATION OF STRESS-CORROSION CRACKS	58
CONCLUSIONS	60
REFERENCES	61
APPENDIX A	63
APPENDIX B	67

LIST OF TABLES

	<u>Page</u>
Table I. Variable Nomenclature for Two-Level Factorial Design	8
Table II. Composition of Aluminum Alloys to be Used to Study Metallurgical Variables	9
Table III. Schedule of Heat Treatment of Al-Zn-Mg Alloys	10
Table IV. Long-Transverse Tensile Properties of Experimental Alloys (0.065-Inch Sheet)	11
Table V. Stress-Corrosion-Cracking Endurance	15
Table VI. Stresses Normal to the Grain Boundary	17
Table VII. Stress-Corrosion-Cracking Endurance	21
Table VIII. Significant Variable Effects	24
Table IX. Data Compiled From Stress-Corrosion-Cracking-Kinetic Studies . .	30
Table X. Results of Electrochemical Studies	35
Table XI. Data for Different Conditions in Autoradiographic Studies	37

LIST OF ILLUSTRATIONS

Figure 1. Fractional Two-Level Factorial Design for Seven Variables . . .	7
Figure 2. Short-Transverse Specimen	12
Figure 3. Uncorrected Effect of Stress Level on Stress-Corrosion- Cracking Endurance	18
Figure 4. Degree of Coincidence of Data Adjusted to 30 Ksi	19
Figure 5. Effect of Direction of Stress Application	22
Figure 6. Effect of the Addition of Silver on Stress-Corrosion- Cracking Behavior	23
Figure 7. Load-Cell Compressing Legs of a Cracked, Short- Transverse Specimen	25
Figure 8. Stress-Corrosion-Cracking Kinetics	28

LIST OF ILLUSTRATIONS
(Continued)

	<u>Page</u>
Figure 9. Oscilloscope Trace (50 Seconds) Showing Continuous Decrease in Strain	29
Figure 10. Surface Appearance of Groove of Short-Transverse Specimen . .	31
Figure 11. Surface of Specimen 3 From Table 10 After Cracking	34
Figure 12. Cross Sections of Specimen 3 From Table 10 After Cracking, Showing That Cracks Progress Faster Below the Surface Than on the Surface	34
Figure 13. Electrochemical Measurement Apparatus	36
Figure 14. Schematic Diagram of Electrochemical Measurement Apparatus . .	36
Figure 15. Photomicrographs of Different Exposure Conditions	38
Figure 16. Transmission Electron Micrographs of 7079-Type Alloys	40
Figure 17. Transmission Electron Micrographs of the Ternary Al-Mg-Zn Alloy Prepared in the Indicated Treatments	41
Figure 18. Electron Micrographs of Stress-Corrosion Fracture Faces in the Overaged and Solution-Treated Ternary Al-Zn-Mg Alloy	43
Figure 19. Light and Electron Micrographs of Stress-Corrosion Fracture Face in a Short-Transverse Specimen of the High-Purity 7079 Alloy	45
Figure 20. Electron Micrographs of the Initially Formed Stress-Corrosion Fracture Faces in Three 7079 Alloys	46
Figure 21. Electron Micrograph of the Ternary Al-Zn-Mg Alloy Cathodically Charged in 5 Vol % Arsenic-Saturated H ₂ SO ₄ for 35 Minutes at 0.02 Amp/Cm ²	47
Figure 22. Electron Micrograph of a Ternary Al-Zn-Mg Alloy Cathodically Charged in 1N Na ₂ SO ₄ + 0.1 Percent Sodium Silicate at 2 x 10 ⁻⁴ Amp/Cm ² for 12 Hours	47
Figure 23. Light Micrograph of Fracture Face in the Ternary Al-Mg-Zn Alloy Cathodically Charged to Failure	48
Figure 24. Electron Micrographs of the Fracture Face of the Ternary Al-Mg-Zn Alloy Cathodically Charged to Failure	49
Figure 25. Transmission Electron Micrograph of a Thin Section of the Ternary Al-Mg-Zn Alloy After Cathodic Charging for 2 Seconds . .	51

LIST OF ILLUSTRATIONS
(Continued)

	<u>Page</u>
Figure 26. Electron-Emission Micrographs of the Ternary Al-Mg-Zn Alloy Exposed to Hydrogen-Ion Bombardment for the Indicated Times . . .	52
Figure 27. Electron-Emission Micrograph of the Ternary Al-Mg-Zn Alloy Exposed to Hydrogen Ions for 165 Minutes	52

A FUNDAMENTAL INVESTIGATION OF THE NATURE OF STRESS-CORROSION CRACKING IN ALUMINUM ALLOYS

by

F. H. Haynie, D. A. Vaughan, D. I. Phalen,
W. K. Boyd, and P. D. Frost

INTRODUCTION

Since World War II there has been an ever-increasing demand for higher performance characteristics in aircraft. These demands have been met partially with the use of high-strength aluminum alloys and by designing so that their strength properties are optimized. The increased use of these materials has been accompanied by an increase in service failures by stress-corrosion cracking. Although several alloys and tempers have been developed which have increased resistance to stress-corrosion cracking, these materials do not always meet the design criteria specified for a particular use. One of the problems associated with the development of alloys which meet the design criteria and also are not susceptible to stress-corrosion cracking is that the mechanism of stress-corrosion cracking is not fully understood.

The objective of this research was to study the mechanism of stress-corrosion cracking in the 7039- and 7079-type alloys. Particular effort was devoted to determining the effect of cathodically produced hydrogen on the mechanism of stress-corrosion cracking.

SUMMARY

Existing theories for the mechanism for stress-corrosion cracking were reviewed. The electrochemical mechanism based on existing anodic paths (not strain induced) does not explain the strong stress dependence of the time required for initiation of stress-corrosion cracks, nor does it explain the fact that alloys susceptible to stress-corrosion cracking are not necessarily susceptible to intergranular corrosion. A purely mechanical mechanism is not applicable because cracks can be stopped by cathodically polarizing susceptible materials. The surface-energy mechanism has proved not to be applicable because under conditions where stress-corrosion cracking has time to occur, the stress-grain size relationship predicts a negative surface energy which is impossible. The electrochemical-mechanical mechanism could be applicable if fast fracture steps occur during the cracking process. However, the latter mechanism was proved not applicable because experimental crack-kinetics studies revealed no fast fracture steps, and the rates of cracking were well within the limits predicted by an electrochemical mechanism.

Besides the crack-kinetics studies, the experimental work consisted of metallurgical-variable studies, electrochemical studies, autoradiographic studies, precipitate-phase studies, fracture-face morphology and surface-reaction studies, and

microstress studies. Statistically designed experiments in the metallurgical variable studies showed that stress-corrosion-cracking susceptibility is a function of the stress normal to the grain boundaries rather than the applied stress in high purity 7039- and 7079-type alloys in thin sheet and plate form. Compensation for this effect was made before the statistical significance of other metallurgical variable effects in the experiment was determined. Chromium-alloy additions, silver-alloy additions, solution heat treatment for longer times at higher than normal T6 treatments, overaging, and the combination of silver and overaging or the combination of chromium and the more severe solution heat treatment were all beneficial to the stress-corrosion-cracking resistance of these particular alloys. The addition of copper was detrimental.

The results of the electrochemical studies indicated that cracking occurred in a high-purity ternary Al-Zn-Mg alloy only when the combination of tensile stress, anodic currents, and cathodic currents was present. Cracking did not occur when any one of the three conditions was absent. Autoradiographic studies indicated that hydrogen concentrates at tensile-strained grain boundaries of stress-corrosion-susceptible alloys of the 7039 and 7079 type. Both the results from the electrochemical studies and the results from the autoradiographic studies were based on a relatively few experiments, the primary purpose of which was to develop techniques. However, the consistency of these results as well as results from fracture-face morphology and surface-reaction studies strengthens the belief that cathodically produced hydrogen dissolved in strained grain boundaries is essential to the initiation of stress-corrosion cracks in these alloys.

This work has led to the advocacy of a mechanism for the initiation of stress-corrosion cracks in these alloys. This mechanism involves the absorption of cathodically produced hydrogen into strained, mechanically weak (alloy-depleted zones) grain boundaries. The hydrogen acts to reduce the activation energy for anodic dissolution of the metal and thus accelerates the localized corrosion at the grain boundaries perpendicular to applied tensile stresses.

REVIEW OF THEORY

The various previously proposed theories for the mechanism of stress-corrosion cracking range from purely mechanical mechanisms to purely electrochemical mechanisms. Modifications and combinations of these two basic mechanisms have evolved to make them more consistent with the observed behavior of stress-corrosion cracking. The four theories that will be discussed are (1) the electrochemical theory, (2) the mechanical theory, (3) the electrochemical-mechanical theory, and (4) the surface-energy theory.

The Electrochemical Theory

Many of the phenomena associated with stress-corrosion cracking can be explained by an electrochemical mechanism. This theory is based on the assumption that the material must be susceptible to selective corrosion along more or less continuous paths, and a condition of sustained tensile stress on the surface must be acting in a

A FUNDAMENTAL INVESTIGATION OF THE NATURE OF STRESS-CORROSION CRACKING IN ALUMINUM ALLOYS

by

F. H. Haynie, D. A. Vaughan, D. I. Phalen,
W. K. Boyd, and P. D. Frost

INTRODUCTION

Since World War II there has been an ever-increasing demand for higher performance characteristics in aircraft. These demands have been met partially with the use of high-strength aluminum alloys and by designing so that their strength properties are optimized. The increased use of these materials has been accompanied by an increase in service failures by stress-corrosion cracking. Although several alloys and tempers have been developed which have increased resistance to stress-corrosion cracking, these materials do not always meet the design criteria specified for a particular use. One of the problems associated with the development of alloys which meet the design criteria and also are not susceptible to stress-corrosion cracking is that the mechanism of stress-corrosion cracking is not fully understood.

The objective of this research was to study the mechanism of stress-corrosion cracking in the 7039- and 7079-type alloys. Particular effort was devoted to determining the effect of cathodically produced hydrogen on the mechanism of stress-corrosion cracking.

SUMMARY

Existing theories for the mechanism for stress-corrosion cracking were reviewed. The electrochemical mechanism based on existing anodic paths (not strain induced) does not explain the strong stress dependence of the time required for initiation of stress-corrosion cracks, nor does it explain the fact that alloys susceptible to stress-corrosion cracking are not necessarily susceptible to intergranular corrosion. A purely mechanical mechanism is not applicable because cracks can be stopped by cathodically polarizing susceptible materials. The surface-energy mechanism has proved not to be applicable because under conditions where stress-corrosion cracking has time to occur, the stress-grain size relationship predicts a negative surface energy which is impossible. The electrochemical-mechanical mechanism could be applicable if fast fracture steps occur during the cracking process. However, the latter mechanism was proved not applicable because experimental crack-kinetics studies revealed no fast fracture steps, and the rates of cracking were well within the limits predicted by an electrochemical mechanism.

Besides the crack-kinetics studies, the experimental work consisted of metallurgical-variable studies, electrochemical studies, autoradiographic studies, precipitate-phase studies, fracture-face morphology and surface-reaction studies, and

direction tending to pull the metal apart along these paths^{(1)*}. The action of stress during the propagation stage is more easily visualized than it is during the initiation stage. Stress concentration at the root of a crack strains the metal beyond the yield point, breaks any protective oxide film that may have formed, and exposes the anodic basis metal to the corrosive environment. ⁽²⁾ The "cracks" should grow principally in a direction perpendicular to the effective maximum tensile stress but may be restricted to either zones of weakness or highly anodic paths or both.

Zones of weakness and preferred anodic paths may result from microsegregation of solute atoms. More complete segregation results in the formation of separate phases. These conditions are present in alloys that are susceptible to intergranular corrosion in the absence of stress. However, in recent years it has been noted⁽³⁾ that materials susceptible to stress-corrosion cracking are not necessarily susceptible to intergranular corrosion. This leads to the conclusion that susceptible anodic paths in these materials result from the action of sustained tensile stresses.

Alloy systems which form passive films and may be pitted in certain environments are generally susceptible to stress-corrosion cracking in those environments. This generalization has led some investigators^(4, 5) to believe that the initiation stage is the process of breaking down the passive film. The localized breakdown of the passive film exposes anodic basis metal and creates a high cathode-to-anode area ratio. The rupture of the passive film may be caused by reaction with the environment (pitting corrosion) or by the mechanical action of stress. In the first case, the time required to form pits can partially explain the observed "incubation" period for the initiation of stress-corrosion cracks. In the second case, if the stress is high enough to rupture the oxide film, initiation should occur immediately. If the stress is not high enough to rupture the film, cracking should not initiate. Neither case is able to explain the strong stress-dependence of the length of the incubation period associated with the initiation stage of stress-corrosion cracking.

The electrochemical theory fails to explain why materials susceptible to intergranular corrosion do not necessarily stress-corrosion crack, nor why materials susceptible to intergranular stress-corrosion cracking are not necessarily susceptible to intergranular corrosion in the absence of stress. The theory is not consistent with the strong stress dependence of the "incubation" period associated with the initiation of stress-corrosion cracks.

The Mechanical Theory

The initiation and propagation of stress-corrosion cracks by purely mechanical means may be explained by two separate processes. In fact, many proponents of the mechanical theory concede that the initiation stage may be an electrochemical reaction. However, mechanical mechanisms by which cracks can initiate will be discussed.

Since the length of the incubation period prior to crack formation is strongly stress dependent, the movement of dislocations may be involved. Dislocations may stack up along slip planes at free surfaces. The accumulated stresses associated with these dislocations should eventually exceed the forces associated with the free surface and cause coarse slip. Swann⁽⁶⁾ has correlated coarse slip with the breakdown of

*References listed at end of report.

protective oxides and the initiation of transcrystalline stress-corrosion cracking. Intergranular cracking may be the result of weak alloy-depleted zones at grain boundaries. Slip would thus be restricted to these zones. Grain-boundary slip then could result in crack initiation at triple points⁽⁷⁾ (intersections of three grain boundaries).

Most materials that are susceptible to stress-corrosion cracking are not normally brittle, although brittle fracture appears to be associated with the phenomenon. Even in relatively brittle metals, plastic deformation on a microscopic scale precedes brittle fracture.⁽⁸⁾ The Orowan modification of Griffith's theory states that the energy required to do plastic work is so much greater than the energy required to create a new surface that new-surface energy can be neglected.⁽⁸⁾ Expressed mathematically,

$$\sigma = \approx \left(\frac{Ep}{c} \right)^{1/2}, \quad (1)$$

where σ is the stress required to start the unstable propagation of a crack, c is the half length of the crack, E is the modulus of elasticity, and p is a plastic-work term.

In a ductile material, the stress concentration at the root of a crack is lowered by local yielding of the material to form a greater root radius. Therefore, the material at the root of the crack must be embrittled before the crack can propagate by a mechanical mechanism. The similarity between hydrogen embrittlement and stress-corrosion cracking suggests that hydrogen, as a corrosion product, may diffuse into the highly strained metal ahead of a crack and cause the otherwise ductile material to become brittle.⁽⁹⁾

The purely mechanical mechanism is inconsistent with several observed characteristics of stress-corrosion cracking. The most striking inconsistency is that stress-corrosion cracking can be accelerated by applying an anodic current and stopped by applying a cathodic current. Another inconsistency is that the rate at which mechanical cracking or ductile fracture should occur is much faster than the observed rates for stress-corrosion cracking. These two inconsistencies alone make the purely mechanical mechanism theory for stress-corrosion cracking unacceptable.

The Electrochemical-Mechanical Theory

This proposed mechanism is a combination of the two previously discussed theories. Alternating slow and fast propagation rates are assumed to be by electrochemical and mechanical mechanisms, respectively. Thus, the observed cracking rate is the average of these alternating steps. Edeleanu⁽¹⁰⁾ has observed transgranular stress-corrosion cracking in which cracks passed through heavy slip bands and were generally held up at light ones. The sudden appearance of faint "ghost" cracks usually preceded the gradual creation of obvious cracks generally perpendicular to the applied stress. A slow sidewise motion of cracks along operative slip planes was felt to be by an electrochemical mechanism. Fontana, commenting on this paper, suggested that the observed "ghosts" may be caused by subsurface cracking.

The stopping and starting of mechanical cracking is more easily explained for intergranular stress-corrosion cracking. The fast-propagating crack may be stopped by grain-boundary precipitates or by a change in the angle of the grain boundary with

respect to the direction of the applied force so that the stress normal to the grain boundary is lowered below a level at which the crack can propagate. The slow electrochemical reaction continues the crack through these obstacles until the mechanical mechanism is again favorable.

Engell and Bäuml⁽¹⁰⁾ have presented evidence to support this theory. The intergranular stress-corrosion cracking of mild steel in a boiling calcium nitrate solution was characterized by rapid steps in elongation of the test specimen, which was accompanied by anodic jumps in corrosion potential. Electrode-potential jumps have also been correlated with audible "pops".⁽¹¹⁾ The "pops" were taken to be the cracking sound that should accompany the sudden energy release associated with brittle fracture.

Parkins⁽¹²⁾ has shown that the rapid-elongation steps observed for mild steel at solution boiling temperatures are not necessarily associated with cracking. A constant strain rate stress-strain curve for this material at 115 C shows a discontinuous "saw tooth" yielding phenomenon. He believes that the potential change was due to exposure of fresh metal by the gross yielding of the specimen. However, another explanation for the potential change is possible. Engell and Bäuml⁽¹⁰⁾ noted that "A cloud of gas bubbles emerges from all the cracks every time a new one is formed." The gross yielding of the specimen dislodges hydrogen bubbles from the cracks, which exposes very active metal at the roots of all the cracks. The popping sound may also be attributed to the bursting of hydrogen gas bubbles from cracks.

The electrochemical-mechanical theory can be made to agree with the observed behavior of stress-corrosion cracking of aluminum alloys. Where one part of the theory is not applicable, the other is. Thus, the two parts complement each other only if the applicable characteristics are considered. The combination of theories to make a more consistent theory is similar to including additional terms in an infinite-series equation. A better fit of data may be obtained by including more terms. Thus, there is the possibility that the electrochemical-mechanical theory is in empirical rather than theoretical agreement with observed stress-corrosion cracking behavior.

The best test of this theory may be obtained from crack kinetics data. If the crack-propagation kinetics for high-strength aluminum alloys are discontinuous, i. e., have extremely fast and slow steps, this theory may be applicable. However, if the kinetics are relatively continuous, the theory is not applicable to this alloy system. For this reason, crack-kinetics studies were included in this research program.

The Surface-Energy Theory

The surface-energy mechanism is not applicable to the initiation of stress-corrosion cracks. Therefore, either microcracks must already be present or the cracks must be formed by some other mechanism. While there is no reliable evidence that Griffith cracks exist in unstressed metals, microcracks can be produced by plastic deformation. (8)

This theory is based on the Griffith crack mechanism for brittle fracture. A lowering of the energy required to form a new surface by the adsorption of specific ions should result in a shorter unstable crack length. Coleman et al. (13) have shown that the fracture stress in a corrosive environment has a grain-size dependence which fits

the Petch-Stroh dislocation model for the generation of a crack nucleus for brittle fracture. The slopes from these measured relationships were used to calculate surface energies that were much lower than the surface energy between the metal and its vapor. These results were assumed to be ample evidence that the surface-energy mechanism is applicable to stress-corrosion cracking. It was also postulated that desorption of negative ions when cathodic currents are applied could account for observed electrochemical behavior.

While surface-energy lowering may contribute to stress-corrosion cracking, it is practically impossible to make the theory completely consistent with observed stress-corrosion cracking behavior. The data of Coleman et al. (13) were obtained by a rapid-loading-rate method. Parkins(12) has shown that if the strain rate is low enough for true stress-corrosion cracking to occur, the fracture-stress, grain-size relationship predicts an impossible negative surface energy. He has also shown that the Petch relationship is applicable to ductile tearing as well as brittle fracture.

EXPERIMENTAL WORK

The experimental work consisted of seven phases: (1) metallurgical-variable studies, (2) crack-kinetics studies, (3) electrochemical studies, (4) autoradiographic studies, (5) precipitate-phase studies, (6) fracture-face-morphology and surface-reaction studies, and (7) microstress studies. Each phase of the work was relatively independent of the other phases. However, the same high-purity alloys were used in each case. Thus, the results of these independent experiments should be consistent. While the results of the independent experiments may be consistent with one or more of the several possible mechanisms for stress-corrosion cracking, the possibility that the combined results are consistent with more than one proposed mechanism is much less.

Metallurgical-Variable Studies

The effects of eight variables on the stress-corrosion cracking susceptibility of high-purity 7039- and 7079-type alloys were determined. These variables are chromium, silver, and copper content, stress level, stress direction, solution heat treatment, cold work, and aging treatment. The design of the experiment for seven of these variables is shown in Figure 1, and the variable levels are given in Table I. The blank spaces represent the combination of conditions tested. Only one fourth of the full design was performed so that the amount of testing could be reduced considerably. The effect of stress was determined by performing the experiment at two different stress levels.

The use of a statistically designed two-level factorial experiment makes it possible to vary all the studied variables simultaneously and still have a sample size of half the total number of tested specimens. It is not necessary to hold all but one variable constant in order to study the effect of that one variable. Interaction effects between variables may also be determined by analysis of variance. Appendix A gives an example of the analysis of variance of a factorial design experiment.

Direction	Solution Heat Treatment	Cold Work	Age	With Cr				Without Cr			
				With Ag		Without Ag		With Ag		Without Ag	
				With Cu	Without Cu	With Cu	Without Cu	With Cu	Without Cu	With Cu	Without Cu
Long Transverse	800 4 hr	Yes	240, 48 hr								
			350, 8 hr								
		No	240, 48 hr								
			350, 8 hr								
	860 1/4 hr	Yes	240, 48 hr								
			350, 8 hr								
		No	240, 48 hr								
			350, 8 hr								
Short Transverse	880 4 hr	Yes	240, 48 hr								
			350, 8 hr								
		No	240, 48 hr								
			350, 8 hr								
	860 1/4 hr	Yes	240, 48 hr								
			350, 8 hr								
		No	240, 48 hr								
			350, 8 hr								

FIGURE 1. FRACTIONAL TWO-LEVEL FACTORIAL DESIGN FOR SEVEN VARIABLES

TABLE I. VARIABLE LEVELS FOR TWO-LEVEL FACTORIAL DESIGN

Variable	Level	
	1	0
Chromium	0.2%	None
Silver	0.2%	None
Copper	0.6%	None
Stress direction	Long transverse	Short transverse
Solution heat treatment	880 F - 4 hr	860 F - 1/4 hr
Cold work	5% reduction	None
Age	5 days at room temperature, followed by 48 hr at 240 F	8 hr at 350 F

Casting and Fabrication of Alloys

The experiment shown in Figure 1 requires 32 different combinations of the tested variables. Four different alloy compositions are required. The desired and actual chemical compositions of the alloys used in this study are given in Table II. The alloys with copper and with chromium were already available in sheet and plate form from work performed in fiscal year 1965⁽¹⁴⁾. All of the alloys contained zinc, magnesium, titanium, and aluminum. Hereafter, these alloys will be identified by their composition variables rather than by their complete compositions.

Two alloys were cast which contained silver. One contained only silver in addition to the basic alloy and the other contained copper, chromium, and silver as additions. These alloys were fabricated and heat treated to conform to the experimental design shown in Figure 1 and Table I. The schedule of heat treatment is given in Table III.

Tensile Properties

Long-transverse tensile properties were determined for each material in the 0.065-inch-thick sheet. The results are given in Table IV. A platen-speed of 0.02 inch/minute was used throughout each test until rupture occurred. Stress-strain data were obtained by means of a 1-inch-gage extensometer. Yield strength, proportional limit, and modulus of elasticity were calculated from the stress-strain data.

Analysis of variance showed that most of the effects of the variables studied were insignificant. The large within-sample variation suggests a marked influence of variables not studied in the experimental design. The heat-to-heat variation in zinc and magnesium content was not considered in this experiment, and it is well known that this variable has a strong effect on the strength of this type of alloy. The only variable studied that had a significant effect on the yield strength was the difference in the aging treatments. Aging at the higher temperature reduced the yield strength.

TABLE II. COMPOSITION OF ALUMINUM ALLOYS TO BE USED TO STUDY METALLURGICAL VARIABLES

Alloys	Chemical Composition, weight percent								
	Fe	Si	Cu	Mg	Mn	Zn	Cr	Ti	Ag
With copper	(High-purity 7079-type alloy without chromium)								
Desired	--	--	0.6	3.3	--	4.3	--	0.1	--
Actual	0.01	0.01	0.56	3.09	N.D.*	3.55	N.D.	0.09	N.D.
With chromium	(High-purity 7039-type alloy)								
Desired	--	--	--	3.3	--	4.3	0.2	0.1	--
Actual	0.03	0.01	N.D.	2.93	N.D.	4.55	0.19	0.09	N.D.
With silver	(High-purity 7039-type alloy with silver replacing chromium)								
Desired	--	--	--	3.3	--	4.3	--	0.1	0.2
Actual	0.01	0.01	0.005	3.08	0.005	4.15	0.005	0.11	0.20
With copper, chromium, and silver	(High-purity 7079-type alloy with silver added)								
Desired	--	--	0.6	3.3	--	4.3	0.2	0.1	0.2
Actual	0.05	0.03	0.60	3.23	0.01	4.29	0.21	0.10	0.19

*N.D. = none detected.

Preparation of Specimens

The 0.065-inch-thick materials were machined into 4.5 x 0.5-inch long-transverse specimens. The 0.25-inch-thick materials were machined into short-transverse specimens having the dimensions shown in Figure 2. The shallow groove on the face of this type specimen was designed to produce a uniform tensile stress when the legs of the specimen were compressed. This particular specimen design allowed 1/4-inch or thicker plate to be tested for stress-corrosion-cracking susceptibility in the short-transverse direction.

The long-transverse specimens were hand polished and then buffed with jewelers rouge on a cloth wheel. The shallow grooved surfaces of the short-transverse specimens were only polished with jeweler's rouge on a cloth wheel. Each specimen was washed in a detergent solution, rinsed, immersed for one minute in a strong NaOH solution at room temperature, rinsed, dipped for 5 seconds in concentrated nitric acid, rinsed in distilled water, and wiped with acetone. Thereafter, the specimens were handled with clean cotton gloves.

Duplicate specimens were stressed to each of two levels, 50 and 80 percent of the 0.2 percent offset yield strength for each of the different material conditions. The long-transverse specimens were stressed in constant deflection in four-point-loading jigs. These jigs were painted 6061-T6 aluminum with glass and ceramic loading points to prevent metal-to-metal contact. The deflections required to obtain the desired stresses were calculated by using the following equation:

$$y = \frac{F(3L^2 - 4A^2)}{12 E D}$$

TABLE III. SCHEDULE OF HEAT TREATMENT OF Al-2.4-Mg ALLOYS

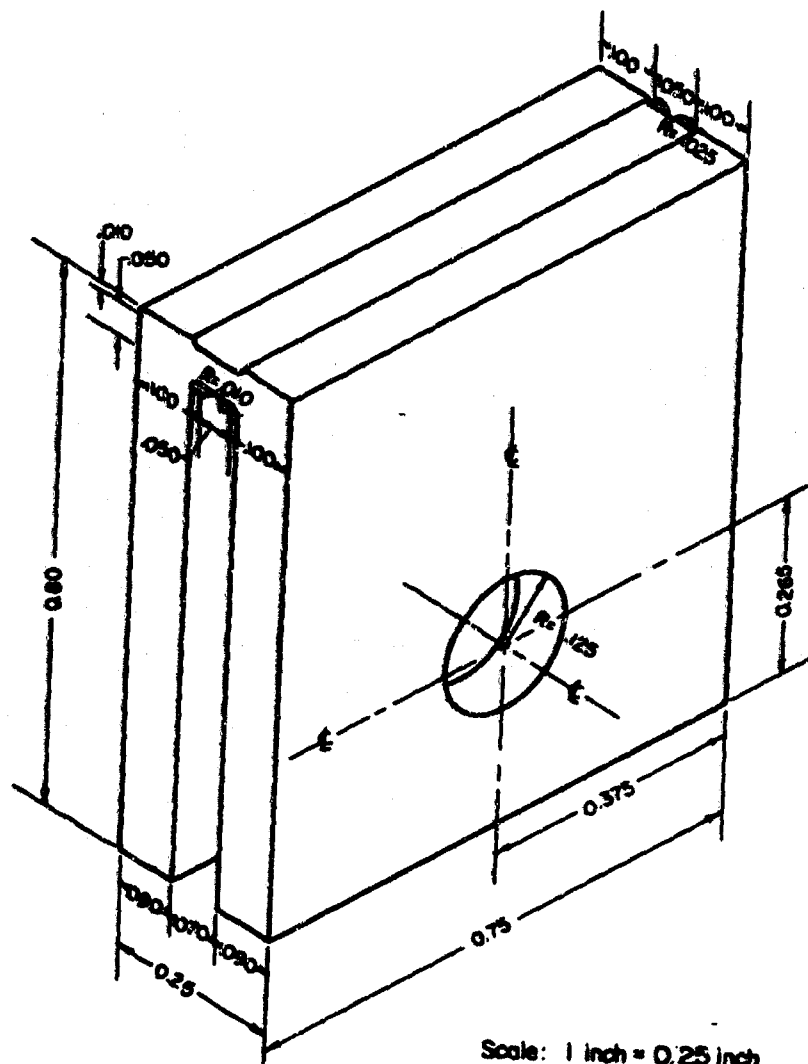
Solution Treat 800 F 4 Hours, Water Quench				Solution Treat 800 F 1 1/4 Hour, Water Quench			
Age 5 Days at Room Temperature - 48 Hr				Age 5 Days at Room Temperature - 48 Hr at 240 F, T-6			
Cold Roll 5 Percent(a)				Cold Roll 5 Percent(a)			
With				With			
Thick- nom. inch	Thick- nom. inch	Alloy	Thick- nom. inch	Thick- nom. inch	Alloy	Thick- nom. inch	Thick- nom. inch
With Cr-Ag-Cu 0.009	With Cr-Ag-Cu 0.009	With Cr	With Ag 0.066	With Ag 0.061	With Ag 0.061	With Cr-Ag-Cu 0.009	With Cr-Ag-Cu 0.009
With Cr-Ag-Cu 0.370	With Cr-Ag-Cu 0.370	With Cr	With Ag 0.370	With Ag 0.260	With Ag 0.260	With Cr-Ag-Cu 0.370	With Cr-Ag-Cu 0.370
With Cu 0.007	With Cu 0.007	With Cu	With Cr 0.063	With Cr 0.063	With Cr (b)	With Cu 0.007	With Cu 0.007
With Cu 0.370	With Cu 0.370	With Cu	With Cr 0.348	With Cr 0.348	With Cr (b)	With Cu 0.370	With Cu 0.370

(a) Cold rolled immediately after solution heat treatment.

(b) Heat treated previously, included for sake of record.

TABLE IV. LONG-TRANSVERSE TENSILE PROPERTIES OF EXPERIMENTAL ALLOYS
(0.065-INCH SHEET)

Alloy	Heat Treatment		Elongation in 1 inch, percent	Yield Strength (0.2% Offset), psi	Tensile Strength, psi	Proportional Limit, psi	Modulus of Elasticity, 10 ⁶ psi
	Solution	Age					
With Cu	880 F 1/4 hr	350 F 8 hr	22	36,600	52,500	25,500	10.8
	880 F 1/4 hr	350 F 8 hr	18	38,000	54,100	31,500	10.1
	Cold rolled 5 percent						
	880 F 4 hr	240 F 48 hr	18	53,200	63,500	43,400	9.8
	880 F 4 hr	240 F 48 hr	12	50,000	64,000	37,300	10.1
	Cold rolled 5 percent						
With Cr	880 F 1/2 hr	240 F 48 hr	8	No curve	86,000	No curve	--
	(Previous heat treatment)		5	82,000	86,000	61,000	9.8
	880 F 1/4 hr	240 F 48 hr	8	80,000	88,000	60,000	9.7
	Cold rolled 5 percent						
	880 F 4 hr	350 F 8 hr	12	59,000	66,500	39,000	10.2
With Cr	880 F 4 hr	350 F 8 hr	14	55,000	64,000	40,000	9.9
	Cold rolled 5 percent						
With Cr-Ag-Cu	880 F 4 hr	240 F 48 hr	7	72,500	80,200	59,000	10.45
			9	71,500	80,200	56,500	10.1
	880 F 4 hr	240 F 48 hr	12	72,000	80,000	53,000	10.3
	Cold rolled 5 percent		9	73,000	80,000	55,000	10.0
	880 F 1/4 hr	350 F 8 hr	9	50,900	65,000	39,800	10.5
			9	49,000	64,300	39,800	10.0
	880 F 1/4 hr	350 F 8 hr	10	46,400	61,500	31,400	10.1
	Cold rolled 5 percent		8	46,400	60,500	29,000	9.9
With Ag	880 F 4 hr	350 F 8 hr	12	51,500	60,000	38,500	10.1
			12	55,000	63,000	35,500	10.4
	880 F 4 hr	350 F 8 hr	12	50,000	59,500	38,500	10.0
	Cold rolled 5 percent		12.5	52,000	61,500	40,000	9.5
	880 F 1/4 hr	240 F 48 hr	77	66,000	72,000	55,500	9.7
			7	No curve	71,900	No curve	--
	880 F 1/4 hr	240 F 48 hr	9	70,000	75,500	50,300	10.5
	Cold rolled 5 percent		9	68,000	74,000	51,000	9.8



Scale: 1 inch = 0.25 inch

A-49401

FIGURE 2. SHORT-TRANSVERSE SPECIMEN

where

y = deflection in inches

F = desired stress, psi

L = beam length in inches (3.68)

A = distance between inner and outer load points
in inches (1.34).

E = Modulus of elasticity in psi (assumed to be
 10.4×10^6 for all alloys)

D = specimen thickness in inches (measured for
each specimen).

A relationship between strain on the grooved surface and the deflection at the ends of the legs was determined for the short-transverse-type specimen with the use of strain gages. With this information and a typical stress-strain curve for this type alloy system, the relationship between stress and deflection to produce stresses at 50 and 80 percent of the yield strength was determined. This relationship was

$$y = K F,$$

where

y = deflection at the ends of the legs in inches

F = desired stress in psi

$K = 3.9 \times 10^{-7}$ and 4.0×10^{-7} for 50 and
80 percent, respectively.

These specimens were then stressed by compressing the legs with nut- and -bolt fittings. The deflections were measured to within 0.001 inch. All but the face of each short-transverse specimen was isolated from the solution with a fast-drying rubber-base coating.

Stress-Corrosion Testing Procedure

A total of 128 specimens were subjected to alternate immersion (10 minutes in and 50 minutes out) in 3.5 percent NaCl solution. The solution was made from distilled water and reagent-grade NaCl. During the period out of solution the specimens were forced-air dried. Distilled water was added periodically during the rest period to make up evaporation losses.

During the first week of exposure the specimens were examined several times a day. During the remainder of the first month they were examined daily. Thereafter the examinations were less frequent. The time of observation of the first sign of a crack was recorded for each failed specimen. Long-transverse specimens were examined visually while the short-transverse specimens were checked with a 30X binocular microscope.

The results are given in Table V. Many of the specimens had not failed during the test period, which obviated the use of standard mathematical analysis-of-variance techniques shown in Appendix A. Booth and Tucker⁽¹⁵⁾ have suggested that stress-corrosion cracking endurance has a log-normal distribution. If such is the case, analysis of variance may be accomplished by plotting the log endurance as a function of the expected probability. The expected probability is based on the number of specimens tested at each level and the ranking of a particular failed specimen. The probability that any one specimen in a sample of 64 will be the first to fail is 1/64. Since it is assumed that expected probability is equivalent to some function of the log endurance, the first specimen should fail some time during the period from 0 to a time equivalent to 1/64 probability. The median of this period represents the best estimate of the time to failure of the first specimen or at 1/128 probability. The best estimates of the probabilities of subsequent failures are

$$\text{Probability} = \frac{1}{128} + \frac{N - 1}{64},$$

where N is the ranking of the particular failure.

Results

The Effect of Stress. The applied stress levels to which the specimens were subjected varied from 16 to 65 ksi. Thus there were actually many more than the two stress levels needed in the factorial design. However, for each material there was a "high" and a "low" stress based on 80 and 50 percent of the yield strength, respectively. Before the effects of all the other variables could be determined, the effect of stress had to be established and the endurance values adjusted to a common stress level.

Prestley⁽¹⁶⁾ has worked with a two-dimensional mathematical model which shows that the effect of specimen orientation on the resistance to stress-corrosion cracking of aluminum alloys is due to the alignment of elongated grains. This idea has been expanded to a three dimensional model.

It was hypothesized that stress-corrosion-cracking susceptibility is a function of the stress normal to the grain boundaries rather than the stress applied to the specimen. The normal stress can be determined if the grain shape and the applied stress are known. It was assumed that an elongated octahedral structure approximates the grain shape. The applied stresses on each material were known. Based on a force balance on the assumed grain shape (Appendix B), the relationship between normal stress and applied stress is

$$\frac{\text{Normal stress}}{\text{Applied stress}} = \frac{b^2 c^2}{a^2 b^2 + c^2 (a^2 + b^2)},$$

where a, b, and c are the relative dimensions of the grain axes. The a-dimension is parallel to the applied stress.

Photomicrographs were made for representative conditions for each experimental alloy in the factorial-design experiment. The average grain dimensions were determined from 10 to 30 measurements in each direction. From these average grain

TABLE V. STRESS-CORROSION-CRACKING ENDURANCE BASED ON FIRST VISUAL SIGN OF A CRACK

Direction	Solution Heat Treatment	Cold Work 5 Percent	Age	Time to Observation of First Crack, hours											
				With Cr-Ag-Cu Stress		With Cr Stress		With Ag Stress		With Cu Stress		High	Low	High	Low
				High	Low	High	Low	High	Low	High	Low				
Long transverse, test time to date - 3120 hr	880 F, 4 hr	Yes	240 F, 48 hr	1960X	NF									28	NF
				NF	NF									43	NF
		No	350 F, 8 hr			NF	NF	NF	NF						
						NF	NF	NF	NF						
	860 F, 1/4 hr	Yes	240 F, 48 hr	1840X	NF									272	NF
				2344X	NF									2944	NF
		No	350 F, 8 hr			NF	NF	NF	NF						
						NF	NF	NF	NF						
			240 F, 48 hr			NF	NF	20	20						
						NF	NF	47	1414						
Short transverse, test time to date - 2900 hr	880 F, 4 hr	Yes	240 F, 48 hr	NF	NF									378	378
				NF	NF									1840	NF
		No	350 F, 8 hr			NF	NF	283	NF						
						NF	NF	908	NF					15	1414
	860 F, 1/4 hr	Yes	240 F, 48 hr	20	128									17	225
				43	176									20	NF
		No	350 F, 8 hr			10	668	543	2824						
						59	NF	1597	NF					59	59
			240 F, 48 hr	80	NF									107	2100
				97	NF										
	860 F, 1/4 hr	Yes	350 F, 8 hr			17	249	2824	NF						
						59	535	NF	NF						
		No	240 F, 48 hr			2.5	2.5	8	78						
						2.5	10	14	150						
		Yes	350 F, 8 hr	70	128									43	43
				NF	NF									NF	NF
		No	240 F, 48 hr			2.5	2.5	8	14						
						2.5	2.5	14	198					2.5	2.5
			350 F, 8 hr	NF	NF									2.5	10

X - Failed by exfoliation.
 NF - No failure during the test period.

dimensions and the applied stresses, the approximate stresses normal to the grain boundaries were calculated for each condition. These data are given in Table VI.

At stresses well above the stress-corrosion-cracking endurance limit (stress level below which stress-corrosion cracking will not occur), the log of the stress-corrosion-cracking endurance should be inversely proportional to the stress level. Expressed mathematically,

$$\frac{d \ln t}{d \sigma} = -K,$$

where t is the stress-corrosion cracking endurance, σ is the stress level, and K is a constant. This relationship has been empirically determined by Gruhl⁽¹⁷⁾. It serves as a basis for determining the effect of stress in this experiment.

The stress-corrosion cracking endurance for the "low" and "high" stresses are plotted as separate functions on log-probability paper in Figure 3. If the "low" and "high" stresses were two constant values rather than ranges of values, according to the assumed mathematical basis, the functions should be two parallel straight lines. Because the high and low stress levels are not single values, only a small portion of the two functions are straight lines. The average stresses normal to the grain boundaries for the first nineteen specimens to fail were 22 and 33 ksi for the low and high stress levels, respectively*. Thus, $d \sigma$ in the stress-time equation is 11 ksi. The parallel portions of the functions in Figure 3 show that the low stressed specimens last nine times longer than the high stressed specimens. The natural log of nine is approximately 2.2, which is $d \ln t$ in the assumed relationship. The resulting constant K in terms of the stress difference in ksi is therefore $2.2/11 = 0.2$.

Values for K around 0.2 were used to adjust endurance for the low and high stress levels to correspond to a common stress level of 30 ksi. A perfect correlation would give straight lines that coincide. The closest approach to coincidence was obtained with a value for K of 0.18. The degree of coincidence decreased when values smaller or larger than 0.18 were used.* The degree of coincidence obtained for a value of K of 0.18 is shown in Figure 4.

At stresses near the threshold stress level, actual stress-endurance data deviate from the logarithmic relationship. This behavior accounts for inability to obtain a perfect correlation. The endurance values at the low stress level were further corrected to account for this deviation so that the two lines coincided. This additional correction is therefore the difference between the two lines at the expected probability for the particular ranked failure. The resulting adjusted values of stress-corrosion-cracking endurance at 30-ksi stress normal to the grain boundaries are given in Table VII. These values were used in the analysis of variance of the remaining variables.

Effect of Direction of Stress Application. The adjusted endurance in Table VII for long-transverse and short-transverse specimens were ranked and plotted as a log function of the expected probability. These data are shown in Figure 5. The 95 percent

*Note. In the Eighth Progress Report the first 23 specimens were used to calculate the average stress levels. Thus, values irrelevant to the linear portions of the curves were used. The resulting value of K of 0.26 was used to plot the low and high stress levels at 20 and 40 ksi, respectively, from which a second estimate of K was determined to be 0.33. Since the degree of fit actually diverges with increasing values of K rather than converges as originally expected, the first estimate was better than the second.

TABLE VI. STRESSES NORMAL TO THE GRAIN BOUNDARY

Alloy Condition ^(a)	Applied Stress (50 and 80 Percent of Yield), ksi	Grain Dimensions			Resolved Stress Normal to Theoretical Grain Boundaries ^(b) , ksi
		a, inch	b, inch	c, inch	
With Cu					
LT, CW, OA	20	0.00585	0.00327	0.00682	4
	30				6
LT, OA	20				4
	30				6
LT, SHT, CW	40	0.00840	0.00316	0.00860	4.4
	25				2.8
LT, SHT	25				2.8
	40				4.4
ST, CW, OA	20	0.00385	0.00615	0.01095	13
	30				20
ST, OA	20				13
	30				20
ST, SHT	25	0.0044	0.0064	0.0129	16
	40				26
ST, SHT, CW	25				16
	40				26
With Cr					
ST, SHT, OA	30	0.00135	0.0036	0.0163	26
	45				39
ST, SHT, CW, OA	30				26
	45				39
ST	40				35
	65				57
ST, CW	40				35
	65				57
LT	40	0.0036	0.00135	0.0163	4.6
	65				7.5
LT, CW	40				4.6
	65				7.5
LT, SHT, OA	30				3.4
	45				5
LT, SHT, CW	30				3.4
	45				5
With Cr-Ag-Cu					
LT, OA	25	0.00562	0.002	0.01475	3
	40				4.5
LT, SHT	35				4
	60				6.7
LT, SHT, CW	35				4
	60				6.7
LT, CW, OA	25				3
	40				4.5
ST, SHT, CW	35	0.0021	0.00395	0.00905	26
	60				45
ST, SHT	35				26
	60				45
ST, CW, OA	25	0.00095	0.00355	0.01235	23
	40				37
ST, OA	25				23
	40				37
With Ag					
LT, SHT, OA	25	0.0083	0.00475	0.0101	8
	40				13
LT, SHT, CW, OA	25				8
	40				13
LT, CW	35	0.00825	0.00545	0.00955	17
	55				27
LT	35				17
	55				27
ST, SHT, CW, OA	25	0.006	0.0107	0.0125	16
	40				26
ST, SHT, OA	25				16
	40				26
ST	35	0.0063	0.0135	0.015	26
	55				41
ST, CW	35				26
	55				41

(a) All alloys contain Al-Mg-Zn-Ti with the additions as stated: LT - long transverse, ST - short transverse, SHT - 880 F 4 hr, CW - 5 percent cold rolled, OA - (over aged) 350 F 8 hr. If not otherwise noted the alloys were solution heat treated at 840 F for 1/4 hr and given the T₆ age, consisting of 3 days at room temperature followed by 48 hr at 240 F.

(b) Values calculated from the grain dimensions and the equation in text.

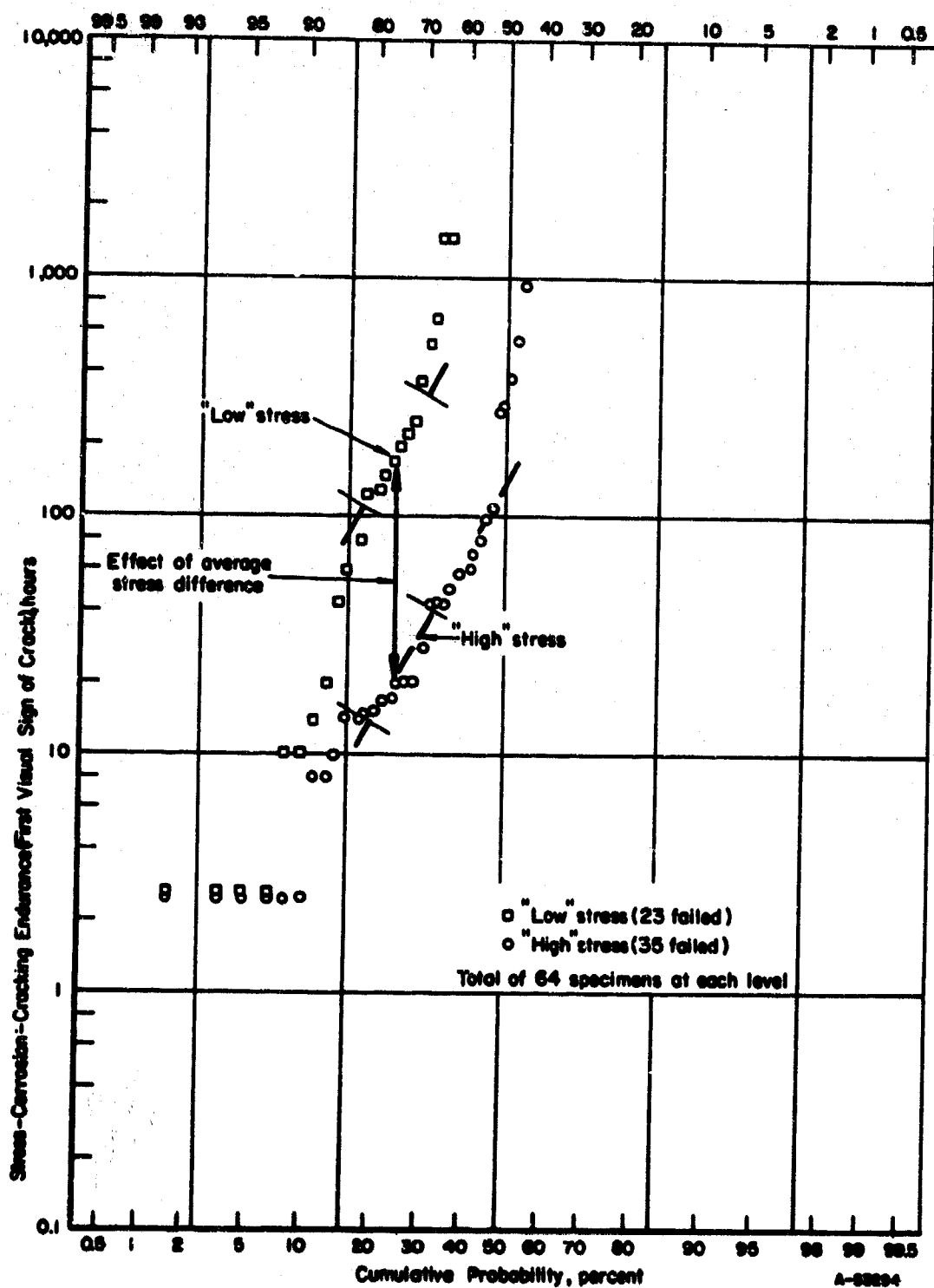


FIGURE 3. UNCORRECTED EFFECT OF STRESS LEVEL ON STRESS-CORROSION-CRACKING ENDURANCE

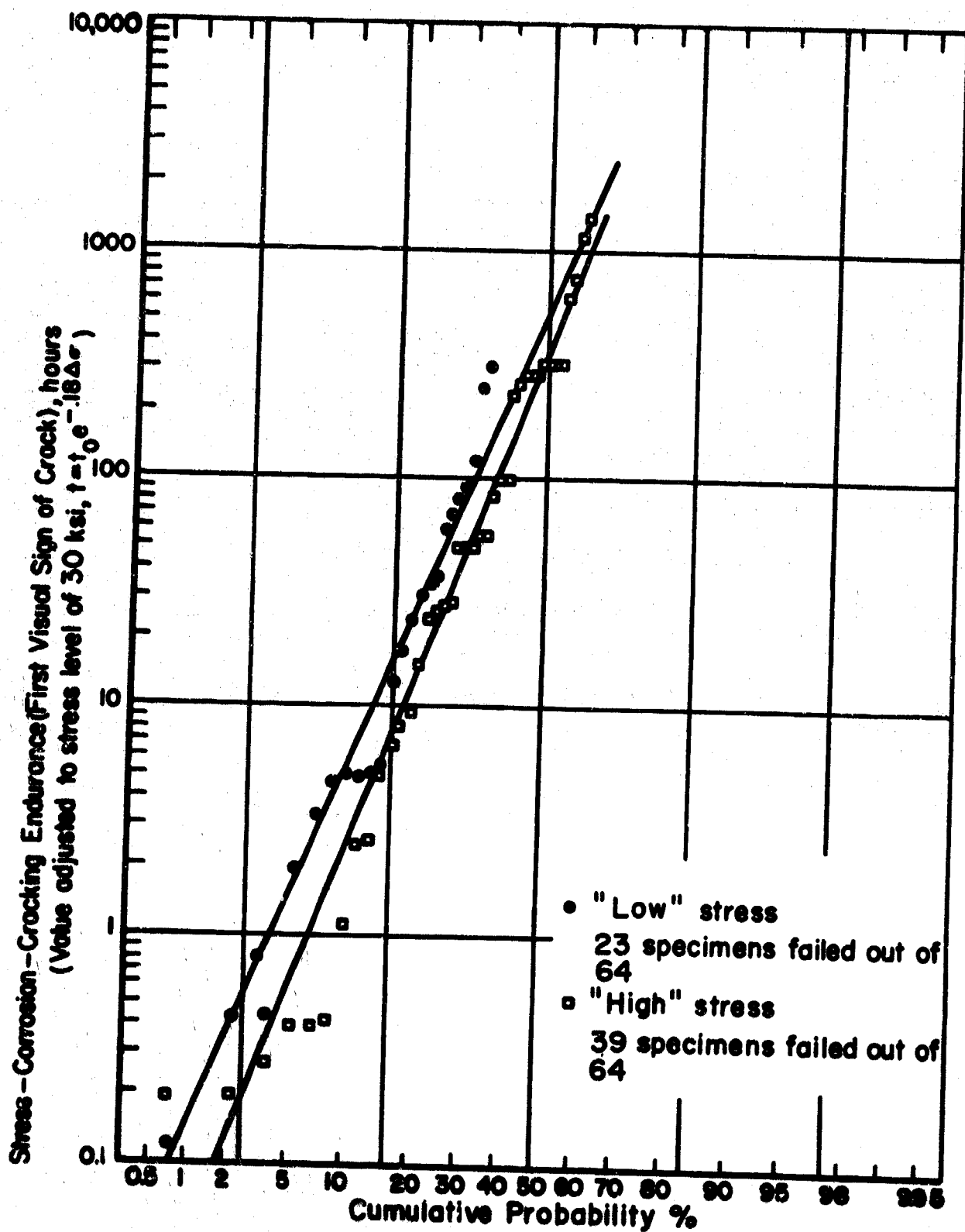


FIGURE 4. DEGREE OF COINCIDENCE OF DATA ADJUSTED TO 30 KSI

confidence limits for the short-transverse specimens were established around the median of the specimens failed rather than the median of the total number of specimens in the sample. However, the standard deviation for the total sample was used. At the median the confidence limits are $\pm ks/\sqrt{n}$, where k is a constant, s is the estimate of the standard deviation, and n is the number of specimens failed. The estimate of the standard deviation is graphically determined from the plot and is the difference between the log endurances at 16.2 and 50 percent probability. The constant k is taken from t tables and is based on the desired confidence and the number of degrees of freedom, which is the number of failed specimens minus one. At plus or minus one standard deviation from the median the limits are expanded by $\pm ks/\sqrt{2n}$. In Figure 5 the endurances for the long-transverse specimens lie well within the 95 percent confidence limits for the short-transverse specimens. Therefore, on the basis of stress normal to the grain boundaries, there is no significant difference in stress-corrosion-cracking susceptibility of specimens stressed in the long-transverse direction and specimens stressed in the short-transverse direction. This behavior supports the original hypothesis that stress-corrosion-cracking susceptibility is a function of stress normal to the grain boundaries rather than the applied stress. It also suggests that the observed differences as a function of stress direction based on the applied stress are related to the grain shape rather than other metallurgical variables. It should be noted that these tests were performed on thin plate and sheet materials. Metallurgical variables which may accompany low cooling rates normally associated with thick sections were not introduced.

Effects of Other Variables and Interactions Between Variables. Analysis of variance was performed on the remaining direct-variable effects and the interaction effects between two variables. Many of these effects proved to be statistically insignificant. However, several of the effects were significant. Figure 6 is an example of the graphical presentation of data of one of these significant effects. Although the 95 percent confidence limits of the two levels overlap (cross-hatched area), the best-fit lines and the data points of the two levels are not mutually inclusive. Therefore, in this example, the addition of silver has a significant beneficial effect. Table VIII gives the pertinent data obtained from similar plots for the significant variables. Variable and interaction-variable effects not listed in this table were found to be insignificant.

Crack-Kinetics Studies

A method was devised by which the cracking kinetics could be studied. This was accomplished by recording the change in strain on load cells (strain-gage-instrumented bolts) compressing the legs of cracking short-transverse specimens (Figure 7). Prior to the stress-corrosion-cracking-kinetics experiments, a correlation was obtained between the depth of a crack and strain on load cells compressing the legs of the cracked specimen.

TABLE VII. STRESS-CORROSION-CRACKING ENDURANCE BASED ON APPLIED STRESSES IN
TABLE VI

Adjusted to 30-Ksi Stress Normal to the Grain Boundaries

Solution Heat Treatment			Endurance, hours					
Direction	Cold Work	Age	With Cr-Ag-Cu		With Cr		With Ag	
			29X	NF	NF	NF	NF	With Cu
Long transverse	880 F, 4 hr	Yes	29X	NF	NF	NF	NF	0.28
								NF
		No	28X	NF	NF	NF	NF	2.7
								NF
	860 F, 1/4 hr	Yes	NF	NF	NF	NF	NF	2.7
								NF
		No	NF	NF	NF	NF	NF	2.6
								NF
Short transverse	880 F, 4 hr	Yes	32	300	50	298	269	0.20
								NF
		No	47	645	181	NF	776	0.20
								NF
	860 F, 1/4 hr	Yes	19	NF	67	145	1380	8.3
								NF
		No	245	NF	86	298	NF	8.7
								NF

X - Failed by exfoliation.

NF - No failure during the test period.

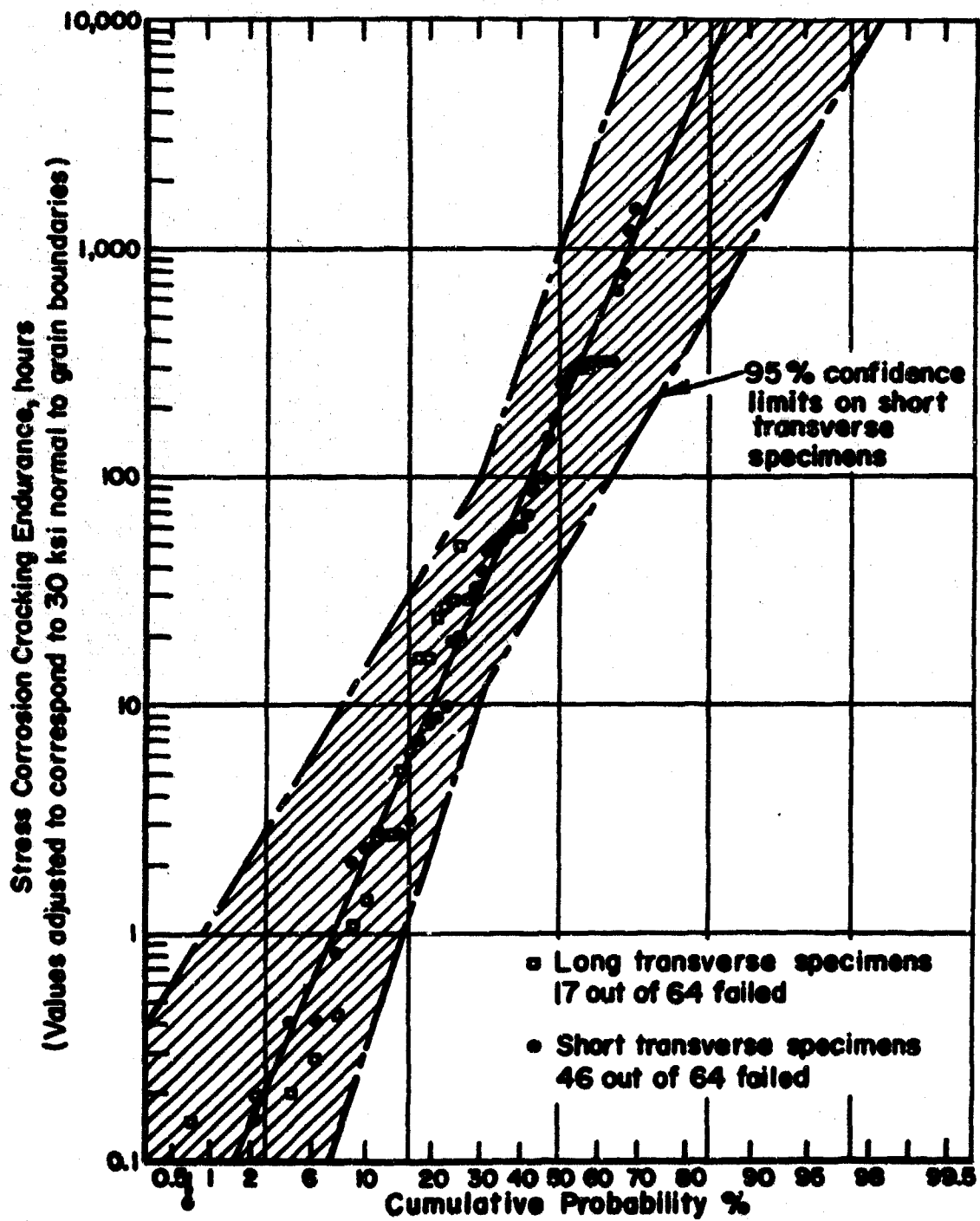


FIGURE 5. EFFECT OF DIRECTION OF STRESS APPLICATION

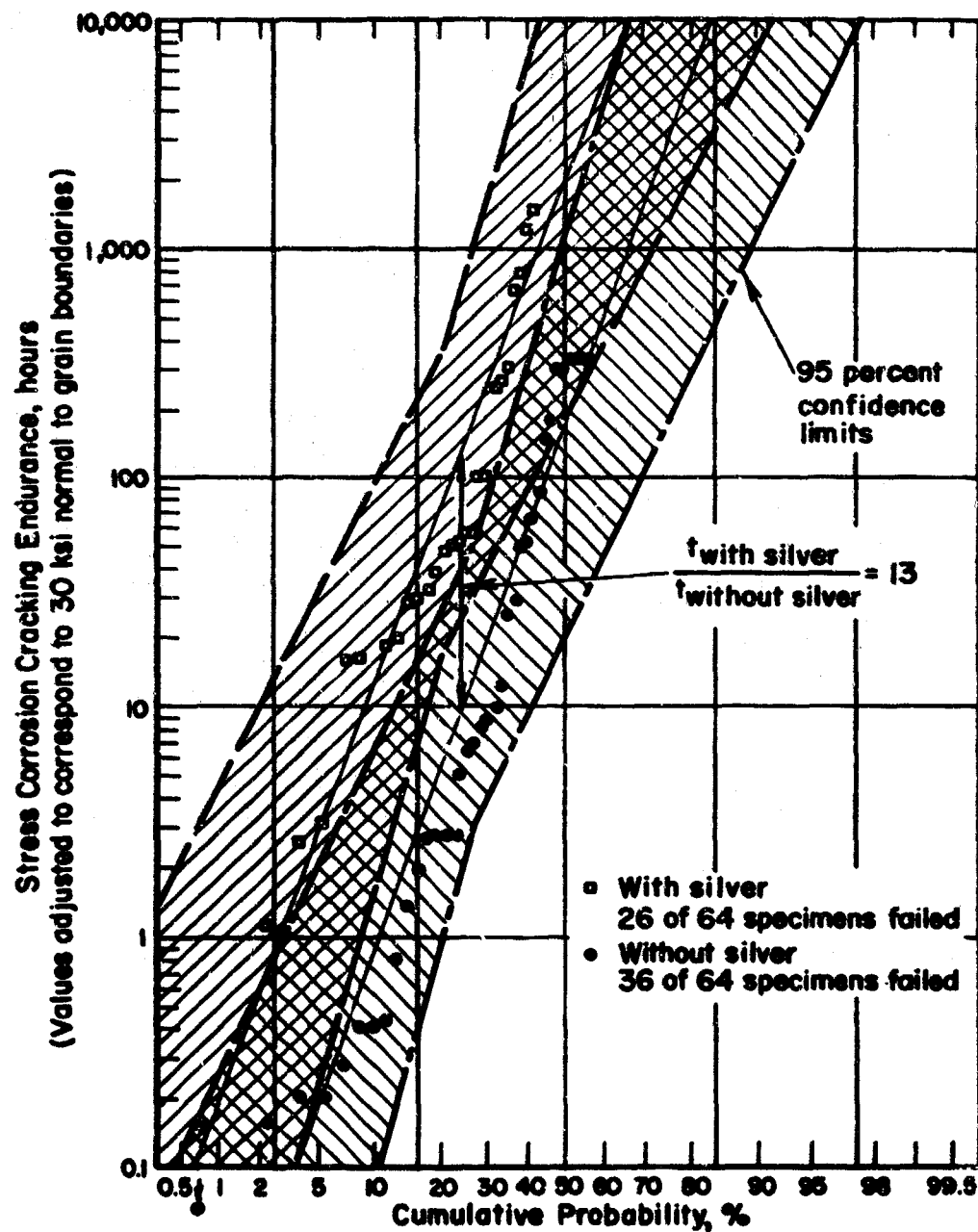


FIGURE 6. EFFECT OF THE ADDITION OF SILVER ON STRESS-CORROSION CRACKING BEHAVIOR

*Confidence limits code




-  Region within 95% confidence limits on best fit line for endurances of alloys containing silver
-  Region within 95% confidence limits on best fit line for endurances of alloys without silver
-  Region common to both

TABLE VIII. SIGNIFICANT VARIABLE EFFECTS

Variable and Level	Endurance, hours		Number of Specimens Failed	Effect
	At Median	- s		
<u>Chromium</u>				
Without	78	2	41	Beneficial
With 0. 2%	1900	80	23	
<u>Silver</u>				
Without	170	2. 7	41	Beneficial
With 0. 2%	2100	39	23	
<u>Copper</u>				
Without	600	23	33	Detrimental
With 0. 6%	380	4	31	
<u>Solution Heat Treatment</u>				
860 F 1/4 hr	150	2. 7	36	Beneficial
880 F 4 hr	2100	46	28	
<u>Age</u>				
240 F 48 hr	240	6. 6	39	Beneficial
350 F 8 hr	5200	15	25	
<u>Interaction Between Chromium and Solution Heat Treatment or Between Silver and Age</u>				
Without Chromium				
860 F 1/4 hr, or	180	3. 3	39	
Without Silver				
240 F 48 hr	3300	39	25	Beneficial
With 0. 2 Cr 880 F				
4 hr, or with	3300	39	25	Beneficial
0. 2 Ag 350 F				
8 hr				

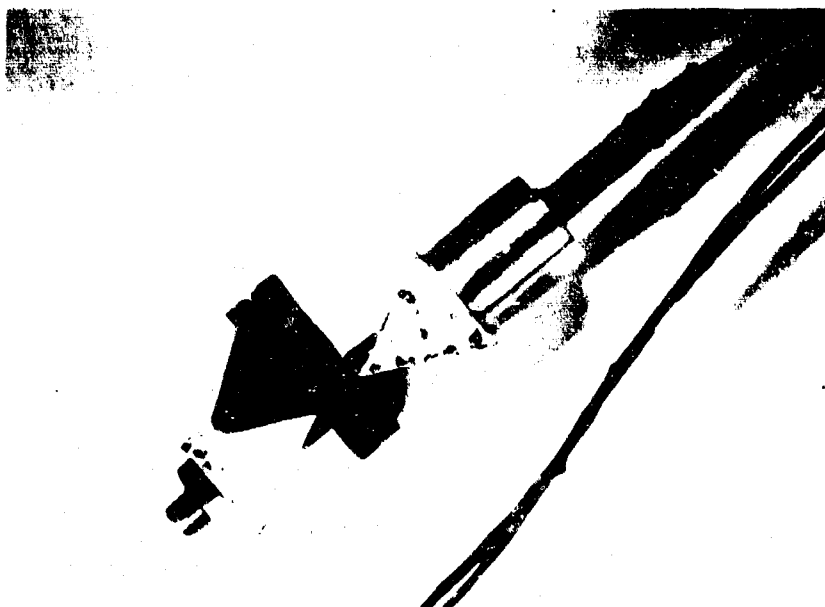


FIGURE 7. LOAD-CELL COMPRESSING LEGS OF A CRACKED, SHORT-TRANSVERSE SPECIMEN

Calibration

Four load cells were numbered one through four. Three short transverse specimens machined from 0.25-inch plate of commercial 7079-T6 alloy were numbered one through three. Specimens were strained by tightening the load cells to deflections of 0.01, 0.02, and 0.03 inch at the load cells. Each specimen was strained in this manner by each load cell, and replicates of six measurements of strain on the load cells were taken. These measurements established that Load Cell 1 was defective and that Load Cells 2, 3, and 4 had different sensitivities. It was also found that different specimens did not affect the strain measurements.

A slot 6 mils wide was cut in the center of the groove of each specimen to a depth of 7 ± 2 mils. Load Cells 3 and 4 were used to strain each specimen. Replicates of six measurements were taken. The slots were deepened to 16 ± 1 mils for Specimen 1 and 28 ± 3 mils for Specimens 2 and 3. Load Cells 2, 3, and 4 were used to measure strain on each specimen. The slots on Specimens 1 and 3 were further deepened to 43 ± 1 and 37 ± 1 mils, respectively. Strains were measured on Specimen 3, using Load Cells 3 and 4. Strains at all deflections of Specimen 1 were too low to measure.

Analysis of variance at slot depths of 0, 7, and 37 mils, deflections of 0.01, 0.02, and 0.03 inch, and Load Cells 3 and 4 showed that slot depth, deflection, and load-cell variables were highly significant. The total interaction of variables was relatively insignificant. These minor interaction effects were probably due to the expected linear dependence of load-cell-difference measurements on strain. That is, the differences between measurements on different load cells are directly proportional to the strain, which is in turn dependent on slot depth and deflection.

The estimated two standard deviations or 95 percent confidence limits are $\pm 34 \mu\text{in. / in.}$ of strain and are independent of the value of strain. The best fit of the data (over 300 measurements), when forced to pass through 0 strain at zero deflection, is given by the following equation:

$$S = \alpha \frac{(50-X)}{50} [D + 8.87D^2 - 355D^3] ,$$

where

S = strain in $\mu\text{in. / in.}$

α = load-cell factor

X = slot depth in mils

D = deflection at the load cell in inches.

The load-cell factors are:

$$\alpha_2 = \text{Load Cell 2} = 6830$$

$$\alpha_3 = \text{Load Cell 3} = 8280$$

$$\alpha_4 = \text{Load Cell 4} = 7170.$$

For a particular deflection and load cell the equation rearranges to give:

$$X = 50 (1 - \alpha \beta S) ,$$

where β is a constant for the deflection effect.

By using the factors for Load Cell 2 and a deflection of 0.032 inch, the results of these data obtained from artificial cracks may be compared with data previously obtained on an actually cracking specimen. (14) The results are:

$$S = 201 \frac{(50-X)}{50} \pm 34$$

for the artificial-crack data, compared with

$$S = 204 \frac{(50-X)}{50} \pm 9$$

as measured on a single stress-corrosion-cracking specimen. The band for the actual-crack data lies well within the confidence limits for the artificial-crack data. Therefore, the strain-crack depth relationship determined from artificial cracks can be used with confidence to measure stress-corrosion crack-growth rates.

Short-transverse specimens were strained by deflecting the legs with a load cell made by inserting a strain gage in a bolt (see Figure 2). The strain on the face of the specimen is proportional to the deflection according to the relationship

$$\epsilon = 330,000y \pm 780$$

where

ϵ = strain, $\mu\text{in.}/\text{in.}$

y = deflection at the load cell, in.

This calibration line was determined by measuring the strain on strain gages mounted in the faces of specimens as a function of deflection.

Results

Five short-transverse specimens (a high purity 7079 T6 alloy) were stressed by compressing the legs with the calibrated load cells. These specimens were placed in a 1N NaCl solution containing 27.6 g/l AlCl_3 with a pH of 3.5. The solution was at room temperature (approximately 74 F). The strain was recorded on an instrument with a full-scale deflection of 1000 $\mu\text{in.}/\text{in.}$ and a chart speed of 4 inches per hour. With the particular load cell used in this experiment, the total change in strain during cracking was approximately 100 $\mu\text{in.}/\text{in.}$ The instrument was insensitive to changes in strain of less than 5 $\mu\text{in.}/\text{in.}$ per inch. Consequently, the cracking kinetics first appeared to proceed in a series of jumps of 5 $\mu\text{in.}/\text{in.}$, indicative of an electrochemical-mechanical mechanism. However, when an oscilloscope was used to determine the rate of these jumps in strain, it was found that the kinetics were fairly slow and continuous and that the jumps were due to the insensitivity of the recording instrument.

Figure 8 shows stress-corrosion-cracking kinetics of short-transverse specimens strained at different levels. Curves 1, 3, 4, and 5 were obtained from strain data using the recording instrument. Curve 2 was obtained from strain data from a timed series of pictures of oscilloscope traces (Figure 9). Calculations of crack depth were based on an unstrained-to-strained deflection of 7.5 cm on the oscilloscope grid. The trace speed was 12 cm/min. Figure 9 is indicative of the continuous nature of the cracking process.

The measured cracking rates and the variables which appear to affect crack kinetics are compiled in Table IX.

Each of the above specimens was observed during the cracking process at 30X. Hydrogen bubbles were observed burating from cracks. This phenomenon was examined in more detail at a higher magnification.

The grooved surface of a short-transverse specimen was buffed with jewelers rouge on a cloth wheel (a metallographic or electrochemical polish could not be used because it would have changed the geometry of the specimen). Some machining scratches were not removed. Figure 10 consists of a series of pictures at 80X. Figures 10a and 10b show the difference in the surface appearance before and after deflecting the specimen 0.030 inch at the bolt. The greater contrast around machining marks in Figure 10b indicated increased plastic flow along these lines. Figure 10c shows the specimen 2 minutes after immersion in 1N NaCl - 27.6 g/l AlCl_3 solution

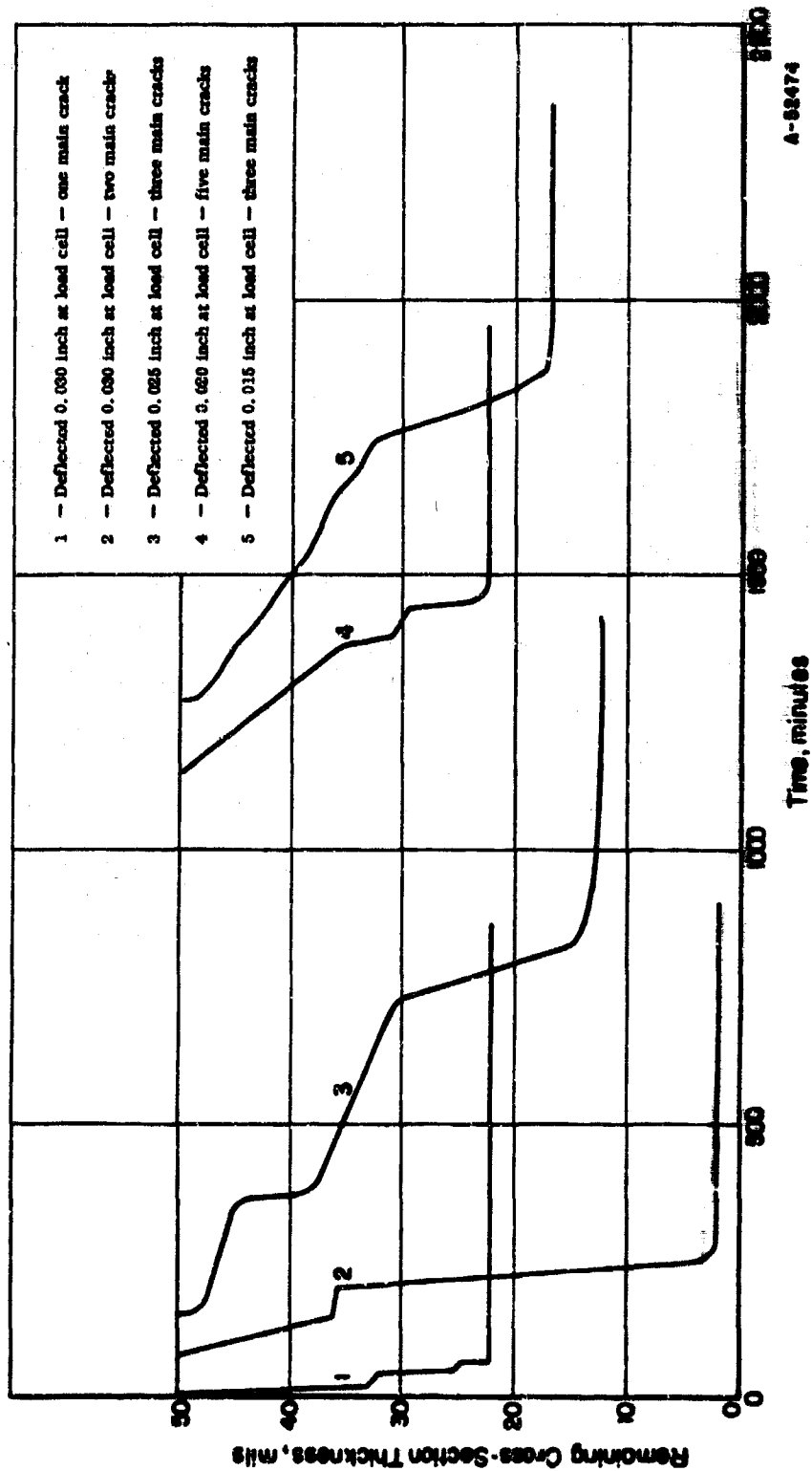
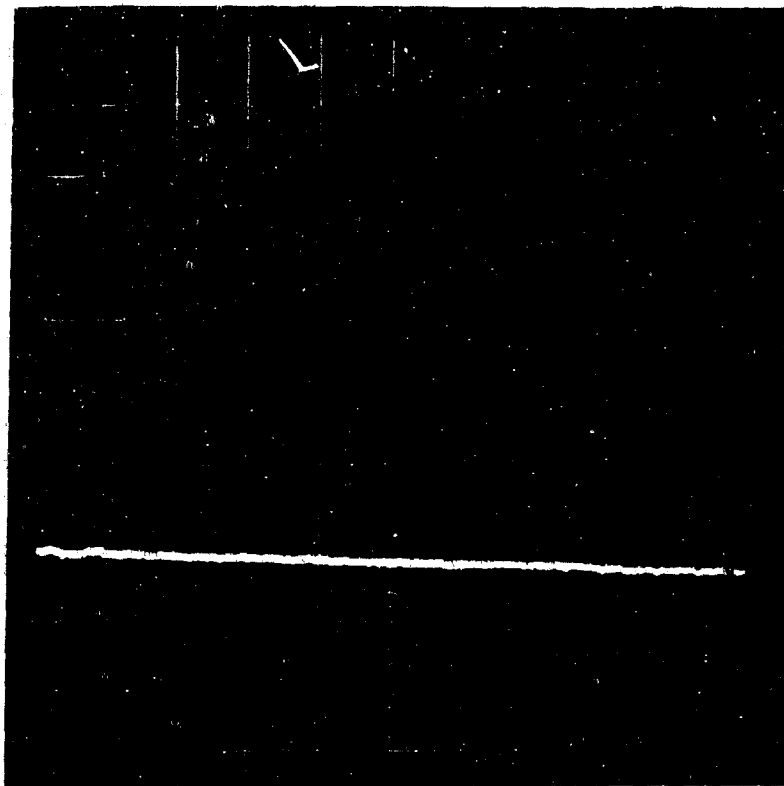


FIGURE 8. STRESS-CORROSION-CRACKING KINETICS

Based on recorded strain on load cell compressing legs of short-transverse specimen.



C2555

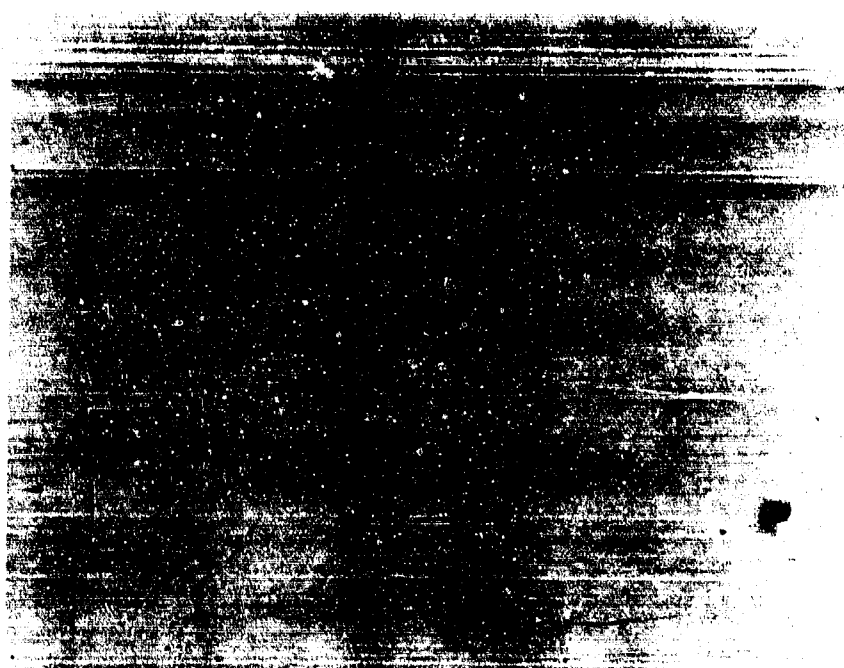
FIGURE 9. OSCILLOSCOPE TRACE (50 SECONDS) SHOWING CONTINUOUS DECREASE IN STRAIN

(pH 3.5). The darkened places were points of corrosion. After the initial attack, there appeared to be no further activity at these points. Figures 10d, 10e, and 10f show the progress of a stress-corrosion crack. In Figure 10d, the crack appears as an S-shape in the center of the bubble. The gray spot just below the bubble is a series of tiny bubbles which evolved during the exposure of the film (approximately 15 seconds). In Figure 10e, the crack has progressed to just below the bubble. Figure 10f shows the appearance of the crack after it has progressed across the picture (taken 46 minutes after exposure). Figure 10g shows that plastic deformation apparently preceded cracking.

TABLE IX. DATA COMPILED FROM STRESS-CORROSION-CRACKING-KINETICS STUDIES

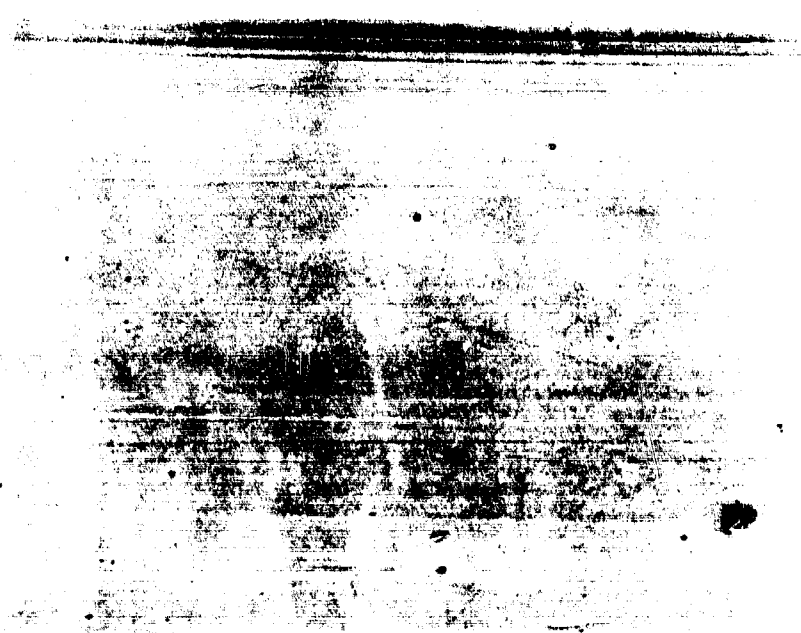
Specimen	Deflection at the Load Cell, in.	Strain Across Short- Transverse Face, $\mu\text{in.}/\text{in.}$	Estimated Stress, 1000 psi	Number of Main Cracks	Time for Initiation, min	Crack Growth Rates, mm/hr
1	0.030	9900 \pm 780	57.5	1	5	1.676 0.108 1.250
2	0.030	9900 \pm 780	57.5	2	90	0.504 1.040
3	0.025	8250 \pm 780	55.0	3	151	0.292 0.038 0.182
4	0.020	6600 \pm 780	47.5	5	577	0.078 0.584 0.076 0.543
5	0.015	4950 \pm 780	42.0	3	1276	0.050 0.204

Figure 11 is a photograph of the face of Specimen 3 from Table IX. Figure 12a is a photograph of a cross section taken at the mark shown in Figure 11. Figure 12b is a photograph of the same general cross section ground down several thousandths of an inch. These two figures show that the cracking progressed faster below the surface than it did on the surface. Thus, it appears that stress-corrosion cracking is favored by the complex state of stress of an internal crack and the local environment within the crack. The plastic deformation which appeared to precede the crack was probably the result of ductile tearing above a subsurface crack.



C2557
 Machine marks
 ↓
 b. After Deflecting Legs 0.030 Inches at Bolt

80X

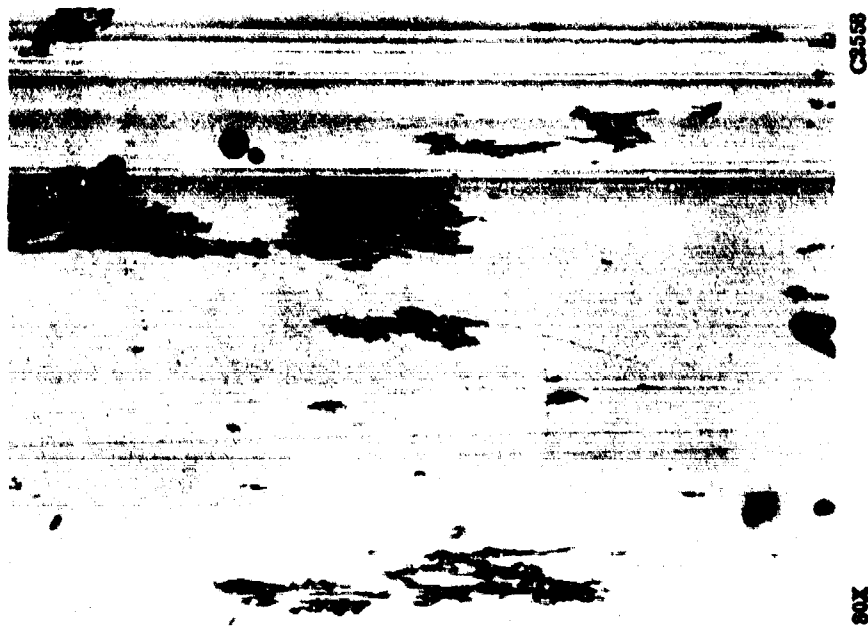


C2556

a. Before Stressing

80X

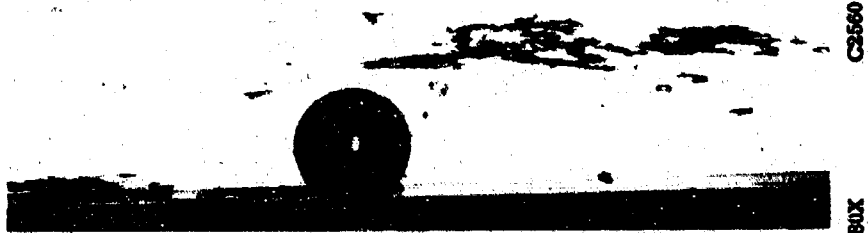
FIGURE 10. SURFACE APPEARANCE OF GROOVE OF SHORT-TRANSVERSE SPECIMEN



c. Two Minutes After Exposure to 1N HCl - 27.6 G/L ANCl₃



d. 13 Min
(Crack initiated.)

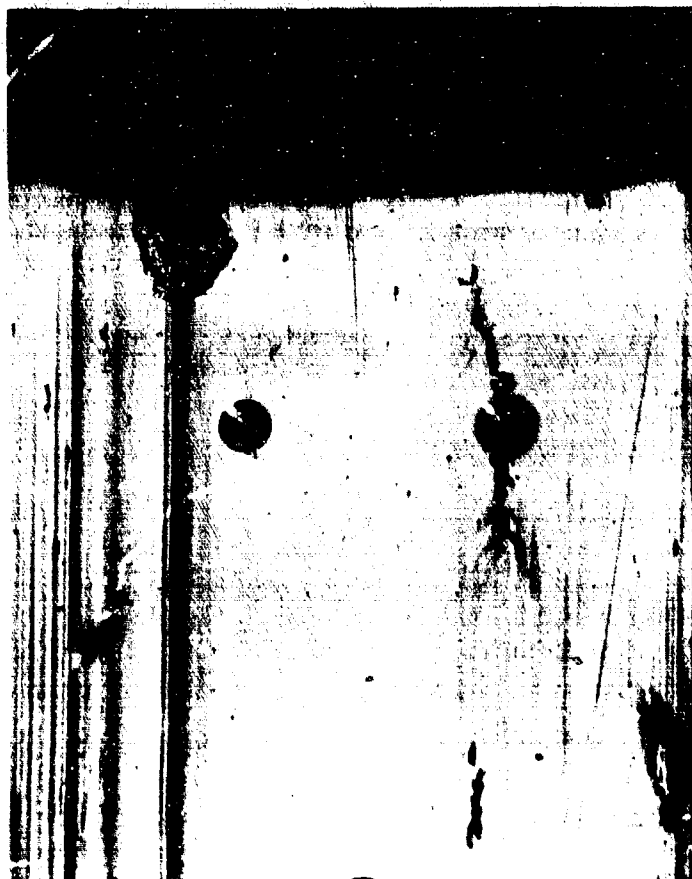


e. 29 Min



f. 46 Min

FIGURE 10. (CONTINUED)

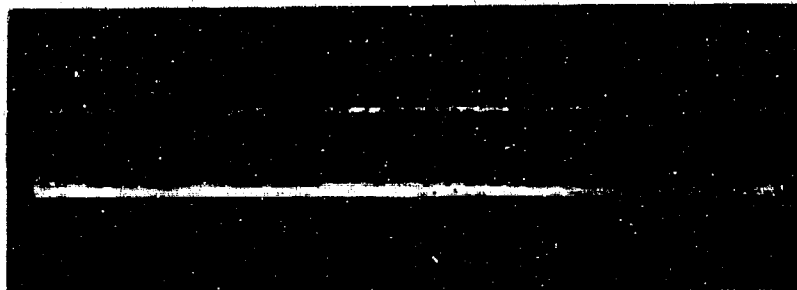


80X

C2562

g. Crack With Plastic Deformation

FIGURE 10. (CONTINUED)



5.5X

CR883

FIGURE 11. SURFACE OF SPECIMEN 3 FROM TABLE 10 AFTER CRACKING



50X Light Kallens' CR884
Etch

a. First Cross Section



50X Light Kallens' CR885
Etch

b. Ground Down 10 Mils

FIGURE 12. CROSS SECTIONS OF SPECIMEN 3 FROM TABLE 10 AFTER CRACKING, SHOWING THAT CRACKS PROGRESS FASTER BELOW THE SURFACE THAN ON THE SURFACE

Electrochemical Studies

An apparatus shown in Figure 13 was designed and constructed which made it possible to separate the effects and interaction effects of anodic and cathodic currents and strain. Figure 14 is a schematic diagram of the apparatus as used in one experiment. One side of a strained sheet tensile specimen could be polarized anodically while the opposite was being polarized cathodically.

A high purity ternary Al-Zn-Mg alloy which is highly susceptible to stress-corrosion cracking was used to study the electrode-kinetics effects. Two basically different types of solutions were used in this study. A one normal sodium sulfate solution inhibited with 0.0005N sodium chromate was selected as a solution that does not normally promote stress-corrosion cracking in this alloy. A 3.5 percent NaCl solution containing 27.6 g/l AlCl_3 adjusted to a pH of 3.5 was selected as a solution that normally causes rapid stress-corrosion cracking.

One side of an unstressed specimen was exposed to the sodium sulfate solution and anodically polarized for 3 hours at -0.500 volt with respect to a Hg-Hg₂SO₄ reference electrode until the current was steady at $1.16 \mu\text{a}/\text{cm}^2$. The corrosive NaCl solution was then placed on the opposite side of the specimen and a constant $116 \mu\text{a}/\text{cm}^2$ of cathodic current was applied to this exposed surface. After 13 hours, the anodic current on the side exposed to the sodium sulfate had increased to $3.48 \mu\text{a}/\text{cm}^2$. The specimen was then stressed in tension to approximately 30 ksi. Within 5 minutes the specimen started to crack.

A second specimen was exposed to anodic polarization in the sodium sulfate solution and stressed in tension to approximately 50 ksi. The opposite side was not exposed to the corrosive salt solution nor the cathodic charging. The specimen did not stress-corrosion crack within 11 hours.

A third specimen was cathodically charged for 17 hours on the side exposed to the corrosive NaCl solution. The specimen was then stressed to approximately 30 ksi. There was no cracking for 23 hours. The sodium sulfate was placed in the opposite cell and that side was polarized anodically. Almost immediately there was an indication of crack initiation. Table X summarizes the combinations of conditions which were tested and the results.

TABLE X. RESULTS OF ELECTROCHEMICAL STUDIES

Anodic Charging	Cathodic Charging	Tensile Stress Applied	Tensile Stress Not Applied
Yes	Yes	Failed	No failure
	No	No failure	No failure
No	Yes	No failure	No failure
	No	Not tested; no failure expected	Not tested; no failure expected

The only failure occurred when stress, anodic charging, and cathodic charging were all present. The significance of these results will be fully covered in the discussion.



FIGURE 13. ELECTROCHEMICAL MEASUREMENT APPARATUS

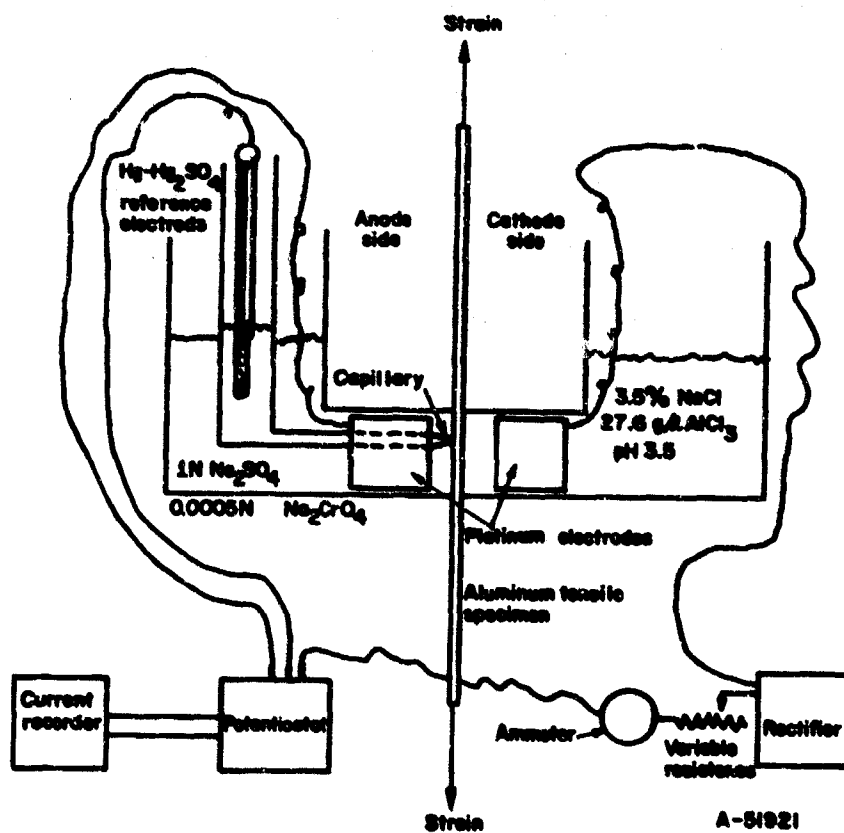


FIGURE 14. SCHEMATIC DIAGRAM OF ELECTROCHEMICAL MEASUREMENT APPARATUS

Autoradiographic Studies to Detect Minute Amounts of
Tritium Absorbed Because of Tensile Stress

Several specimens of a high-purity ternary Al-Zn-Mg alloy, which is susceptible to stress-corrosion cracking, were electropolished in a phosphoric-chromic-sulfuric acid solution. Some specimens were stressed by constant deflection in four-point-loading jigs. Others were not stressed. These specimens were subjected to different exposure conditions. Some specimens were cathodically charged while others were not. Tritiated water was added to some electrolytes.

The electrolyte consisted of 125 ml of 1 N Na₂SO₄. In addition, the radioactive solution contained 100 millicuries (5 ml) of tritiated water.

A summary of the different exposure conditions is given in Table XI. The higher current densities caused caustic attack of the aluminum. Thus, the lower current densities for longer exposure were more satisfactory.

TABLE XI. DATA FOR DIFFERENT CONDITIONS IN AUTORADIOGRAPHIC STUDIES

Condition	Current, ma	Current Density, $\mu\text{a}/\text{cm}^2$	Duration of Electrolysis, hr	Length of Film Exposure, hr
Stressed (40 ksi)	1.5	120	4.5	16
Unstressed	1.5	150	4.5	16
Stressed (40 ksi)	1.25	100	4.5	16
Unstressed	1.0	100	4.5	16
Stressed (40 ksi)	0.65	50	3.5	2, 60
Unstressed	0.5	50	3.5	2, 60
Stressed (40 ksi)	0.65	50	6	3, 60
Unstressed	0.5	50	6	3, 60
Lighter (20 ksi), stressed	0.65	50	6	3, 60
Unstressed	0.5	50	6	3, 60
No H ³ , unstressed	0.5	50	6	2, 60
No H ³ , stressed (40 ksi)	0.65	50	6	3, 60

After exposure to the solution under the various conditions of charging, each specimen was cleaned. A 1-micron film of VYNS (a Bakelite Co. trade designation for a polyvinyl polymer applied in a solution) followed by a 1-micron film of collodion was applied to each specimen to prevent the possibility of the aluminum reacting with the halides in the autoradiographic film. A Kodak Autoradiographic Stripping Plate AR. 10 was then applied to the specimens and exposed for the times indicated in Table XI. The film was developed for 3 minutes in D-19 and fixed for 3 minutes in a Kodak acid fixer.

Figure 15 is typical of the autoradiographs obtained by this method. The four pictures represent four different types of environmental exposure. Pictures a and b show the difference between stressed and unstressed specimens cathodically charged



250X

1A698

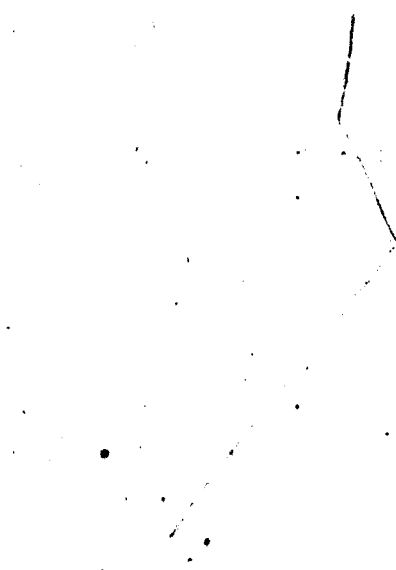


250X

1A702

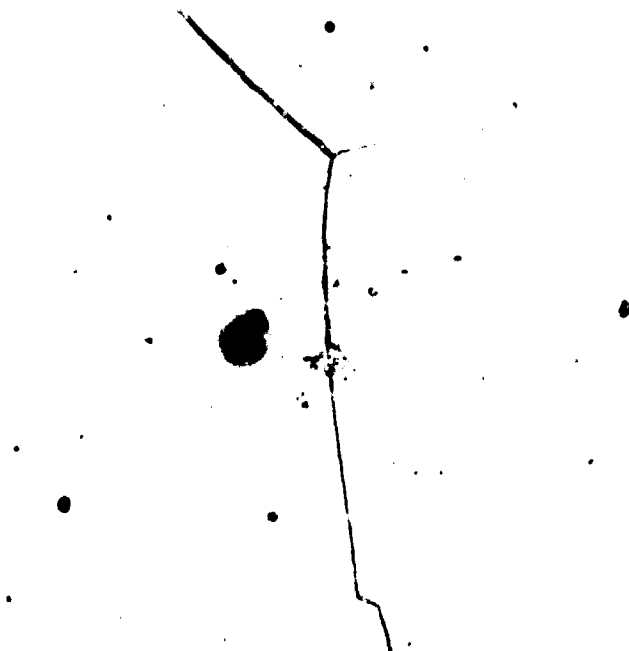
a. Unstressed - Charged in Tritiated Solution for 6 Hours
at $50 \mu\text{a}/\text{cm}^2$ - 60-Hour Film Exposure

b. Stressed 20 Ksi - Charged in Tritiated Solution for 6 Hours
at $50 \mu\text{a}/\text{cm}^2$ - 60-Hour Film Exposure



250X

1A821



250X

1A823

c. Unstressed - Not Charged - 60-Hour Film Exposure

d. Stressed 40 Ksi - Charged 8 Hours in Nontritiated
Solution at $50 \mu\text{a}/\text{cm}^2$ - 60-Hour Film Exposure

FIGURE 16. PHOTOMICROGRAPHS OF DIFFERENT EXPOSURE CONDITIONS

in a tritiated solution. The dark line in b is caused by heavy exposure of the film above a stress-corrosion crack. The small black spots along the grain boundary at the top of the picture are also caused by exposure of the film. Neither of these phenomena is present in the unstressed specimen. Pictures c and d represent controls which were not exposed to tritiated water. A crack is present in picture d; however, heavy exposure of the film above the crack is not evident. The difference between pictures b and d is attributed to the presence of tritium in the grain boundaries of the specimen charged in the tritiated solution. The presence of tritium indicates that hydrogen should be present in even greater concentrations because of the difference in sizes of the two atoms.

The cracking of the specimens was not desired, nor was it expected in a sodium sulfate solution. The cracking behavior was attributed to a decrease in pH of the small volume of solution caused by some cathodic dissolution of the metal. The cracking may have been avoided by using a larger volume of solution and lower current densities or by coating the tensile side of a bent specimen and charging only the compression side. Cracking should be avoided because, if the VYNS film separating the metal from the autoradiographic film is broken the metal will react with the halides in the film and give a false exposure picture similar to picture b. For this reason, it is felt that the black dots along the uncracked grain boundaries are more indicative of the presence of hydrogen than is the dark black line above the crack. The significance of these results will be discussed later.

Precipitate-Phase Studies

Transmission electron micrographs⁽¹⁴⁾ (Figure 16) have shown that both commercial and high purity 7079-T6 alloys contain intragranular as well as intergranular precipitates. The high purity alloy was less susceptible to stress-corrosion cracking in the long-transverse direction than was the commercial-purity alloy. The high-purity alloy contained fewer intergranular precipitates than did the commercial-purity alloy. In all cases, the intergranular precipitate was present as individual particles rather than as a continuous phase in the grain boundary. The major compositional differences between the two alloys were that the high-purity alloy contained less iron and silicon and more chromium than did the commercial purity alloy.

Attempts to identify the precipitate phases by X-ray and electron-diffraction examination of bulk specimens were not successful; hence, transmission-electron-diffraction studies of thin sections were performed. As no intragranular precipitate was present in a ternary Al-Mg-Zn alloy, this alloy was used to investigate the intergranular precipitate. Solution and overaging heat treatments were carried out on specimens of this alloy to decrease and increase, respectively, the amount of the intergranular precipitate phase. Figures 17a, 17b, and 17c are transmission electron micrographs of the ternary Al-Mg-Zn alloy in the following conditions:

- (1) T6 condition
- (2) T6 condition plus a solution treatment of 1 hour at 860 F followed by a cold (60 F) water quench
- (3) T6 condition plus further aging of 1 hour at 350 F, followed by a cold (60 F) water quench.



12,250X

J12835

(a) Commercial Purity 7079-T6



12,250X

J12830

(b) High-Purity 7079-T6

FIGURE 16. TRANSMISSION ELECTRON MICROGRAPHS OF 7079-TYPE ALLOYS

The black dots are due to precipitate phases, while dark bands and lines are due to structural faults.



12, 250X

J12741

a. T6 Treatment



12, 250X

J12841

b. T6 Treatment Plus Solution Treatment,
1 Hour at 880 F



12, 250X

J12790

c. T6 Treatment Plus Overaging 1 Hour
at 350 F

FIGURE 17. TRANSMISSION ELECTRON MICROGRAPHS OF THE TERNARY Al-Mg-Zn ALLOY PREPARED
IN THE INDICATED TREATMENTS

The solution treatment (Figure 17b) decreased the amount of but did not completely remove the intergranular precipitate, while overaging (Figure 17c) increased the width of the grain boundary zone and the size of the intergranular precipitate. The precipitate-free areas adjacent to the larger intergranular precipitates in Figure 17c result from solid-solution depletion as the precipitate grows.

Specimens having these treatments were tested for stress-corrosion cracking behavior under an applied load of 32.4 ksi. The same load was also used in testing other ternary Al-Mg-Zn alloys in the T6 condition, where it represented about 50 percent of the yield strength. Thus, the 32.4-ksi loading of weaker solution-treated and overaged specimens is undoubtedly greater than 50 percent of their yield strength.

Under the 32.4-ksi load, all the cold-water-quenched specimens failed within 167 hours, while hot-water-quenched specimens (all in the T6 condition) failed in from 362 to 1673 hours. [Cracks formed in the overaged specimen (Treatment 3) in less time (84 hours) than in specimens with the T6 treatment.] One of the solution-treated specimens (Condition 2) failed in 800 hours, while another specimen has not failed in a similar exposure time. The endurance time of 800 hours represents a significant improvement over the 167-hour lifetime of specimens in the T6 condition.

Transmission-electron-diffraction data have been obtained for the intragranular precipitate in the high-purity 7079 alloy. However, these data do not correspond to those previously reported for precipitate phases in this type of alloy. A consideration of the solid-solubility relationships between the major elements in 7079 alloys and the available diffraction data for the intermetallic phases present in the appropriate binary and ternary systems suggests that a likely precipitate would be ϵCuZn_4 . Unfortunately, X-ray data obtained from an 80Zn-20Cu alloy did not agree with diffraction data obtained from the 7079 alloy.

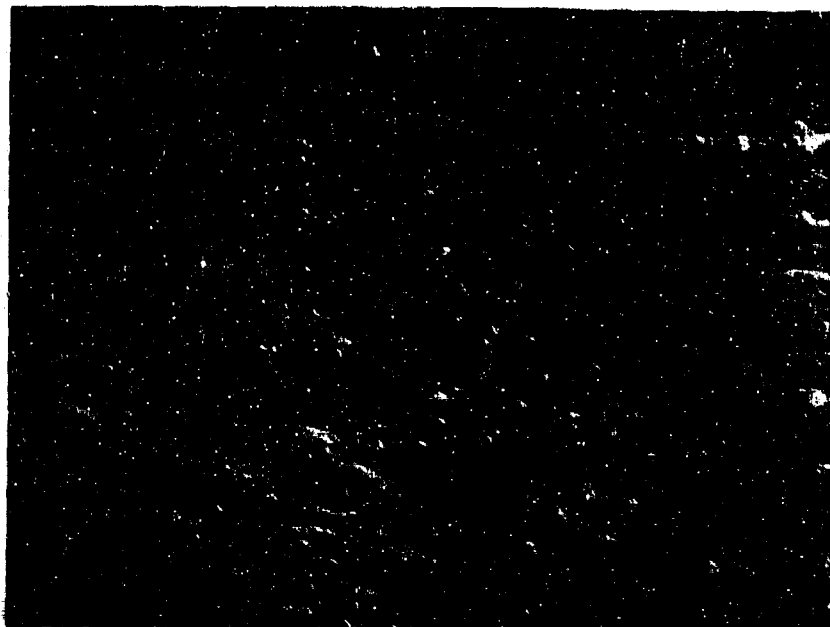
The experimental problems encountered in transmission electron diffraction of thin foils include:

- (1) Limited volume of specimen (very few precipitate particles were available for diffraction)
- (2) The possible interference of surface films.

The significance of these results will be discussed later.

Fracture-Face-Morphology and Surface-Reaction Studies

The fracture-surface morphologies of solution-treated (1 hour at 860 F) and overaged (1 hour at 350 F) ternary Al-Zn-Mg alloys which failed by stress-corrosion cracking in 800 and 167 hours, respectively, were examined. Both fractures were intergranular, but differed in that the fracture face of the overaged specimen (shown in Figure 18a) contained a large number of precipitates, while little evidence of precipitates was observed in the solution-treated alloy (Figure 18b). These results are in agreement with the transmission electron micrographs shown in Figure 17 and further emphasize the observation that intergranular precipitates contribute to grain-boundary weakness and, thus, to stress-corrosion-cracking susceptibility in Type 7079 alloys.



8750X

J13263

a. Overaged 1 Hour at 350 F



8750X

J13314

b. Solution Treated 1 Hour at 860 F

FIGURE 18. ELECTRON MICROGRAPHS OF STRESS-CORROSION FRACTURE FACES IN THE OVERAGED AND SOLUTION-TREATED TERNARY Al-Zn-Mg ALLOY

Experiments have shown short-transverse specimens of the high-purity Type 7079 alloy to be susceptible to stress-corrosion cracking. This alloy does not contain appreciable amounts of intergranular precipitate. Microscopic examination of the fracture face in the short-transverse specimen (Figure 19) showed the fracture to be relatively flat, with small changes in elevation from one grain to another. No definite sequence of structural features across the fracture face was observed. Instead, the rough areas, smooth areas, pits or tunnels, subgrain attack, and steps at grain boundaries were present in varying degrees across the entire fracture face. The flatness of the fracture results from the small orientation difference between adjacent grain boundaries.

The fracture-surface morphology at and near the site of crack initiation was investigated for three materials (Commercial 7079, Al-Mg-Zn-Ti-Cu, and Al-Mg-Zn-Cu) in the T6 condition, after the first evidence of cracking was visible on their exposed surfaces. Electron micrographs obtained by replicating the fracture surface of the cracks are shown in Figures 20a, 20b, and 20c. These fracture surfaces, which are very near the apex of the crack, are quite flat, with pits and tunnels on the grain faces extending into the fracture surface. The pit and tunnel structure is similar to that observed at the apex of cracks of extensively cracked specimens.

Electron-microscopic examination of the ternary Al-Zn-Mg alloy after cathodic charging (Figure 21) indicated that the experimental conditions employed (5 vol % arsenic-saturated H_2SO_4 at 0.02 amp/cm² for 35 minutes) result in localized attack similar to that observed near the apex of a stress-corrosion crack. Less severe conditions (1N Na_2SO_4 inhibited with 0.1 percent sodium silicate at 2×10^{-4} amp/cm²) did not cause tunnels after cathodic charging for 12 hours as can be seen in Figure 22. The observed pits in Figure 22, for this specimen, formed as a result of some etching during the initial electropolishing of the specimen. The background structure, consisting of small bumps which were not present after 35 minutes of charging, suggested the beginning of a surface reaction. A specimen of the ternary Al-Zn-Mg alloy, stressed at 48,000 psi and cathodically charged in the 1N Na_2SO_4 + 0.1 percent sodium silicate electrolyte, showed intergranular cracking in 19 hours.

This suggested that corrosion-produced hydrogen may play a significant role in the stress-corrosion cracking of aluminum alloys. To further define the role of hydrogen in stress-corrosion cracking of 7079 alloys, the effect of atomic hydrogen on the structural properties of these materials was studied.

Hydrogen charging of specimens was accomplished by cathodic treatments in an arsenic-saturated 5 volume percent H_2SO_4 electrolyte at 0.02 amp/cm². The ternary Al-Mg-Zn alloy (susceptible to stress-corrosion cracking) and the high-purity 7079 alloy were cathodically charged while stressed by applied loads equal to 75 percent of their ultimate strength. Intergranular failure in the ternary alloy occurred after approximately 20 hours, while the high-purity alloy stressed in the long-transverse direction showed no cracks after charging for 66 hours. (Stress-corrosion cracking failures without charging are not expected in this solution.)

The grain-boundary fracture path resulting from hydrogen charging is shown in Figure 23 to extend completely across the specimen. The grain-boundary surface is irregular. Electron micrographs illustrating the various types of roughness are presented in Figure 24.

Studies of the effect of hydrogen on internal structures were performed by cathodically charging an unstressed thin section of the ternary Al-Mg-Zn alloy in the T6



50X

L16557

a. Light Micrograph



8750X

J13587

b. Electron Micrograph

FIGURE 19. LIGHT AND ELECTRON MICROGRAPHS OF STRESS-CORROSION FRACTURE FACE IN A SHORT-TRANSVERSE SPECIMEN OF THE HIGH-PURITY 7079 ALLOY



8750X

J12987

a. Commercial 7079



8750X

J12977

b. Al-Mg-Zn-Ti-Cu

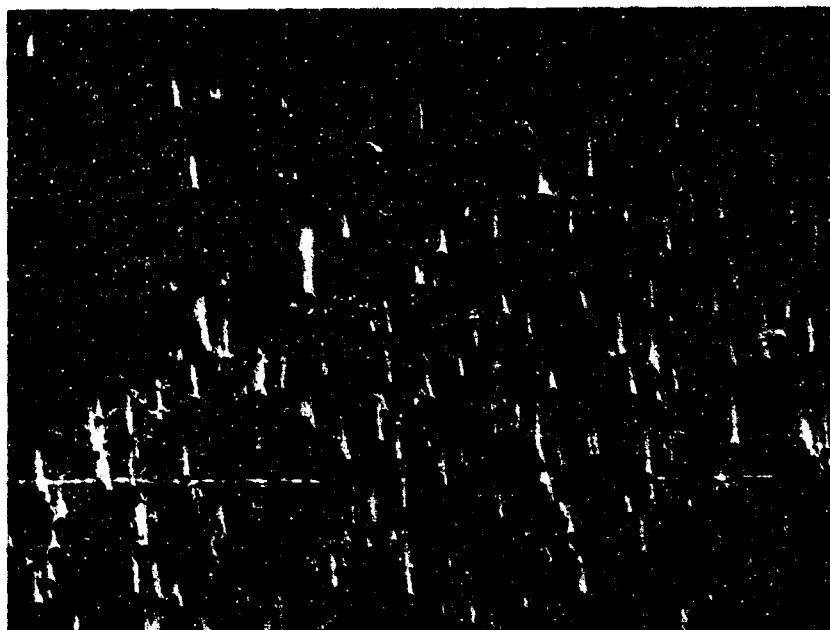


8750X

J12982

c. Al-Mg-Zn-Cu

FIGURE 20. ELECTRON MICROGRAPHS OF THE INITIALLY FORMED STRESS-CORROSION FRACTURE FACES IN THREE 7079 ALLOYS



8750X

J13552

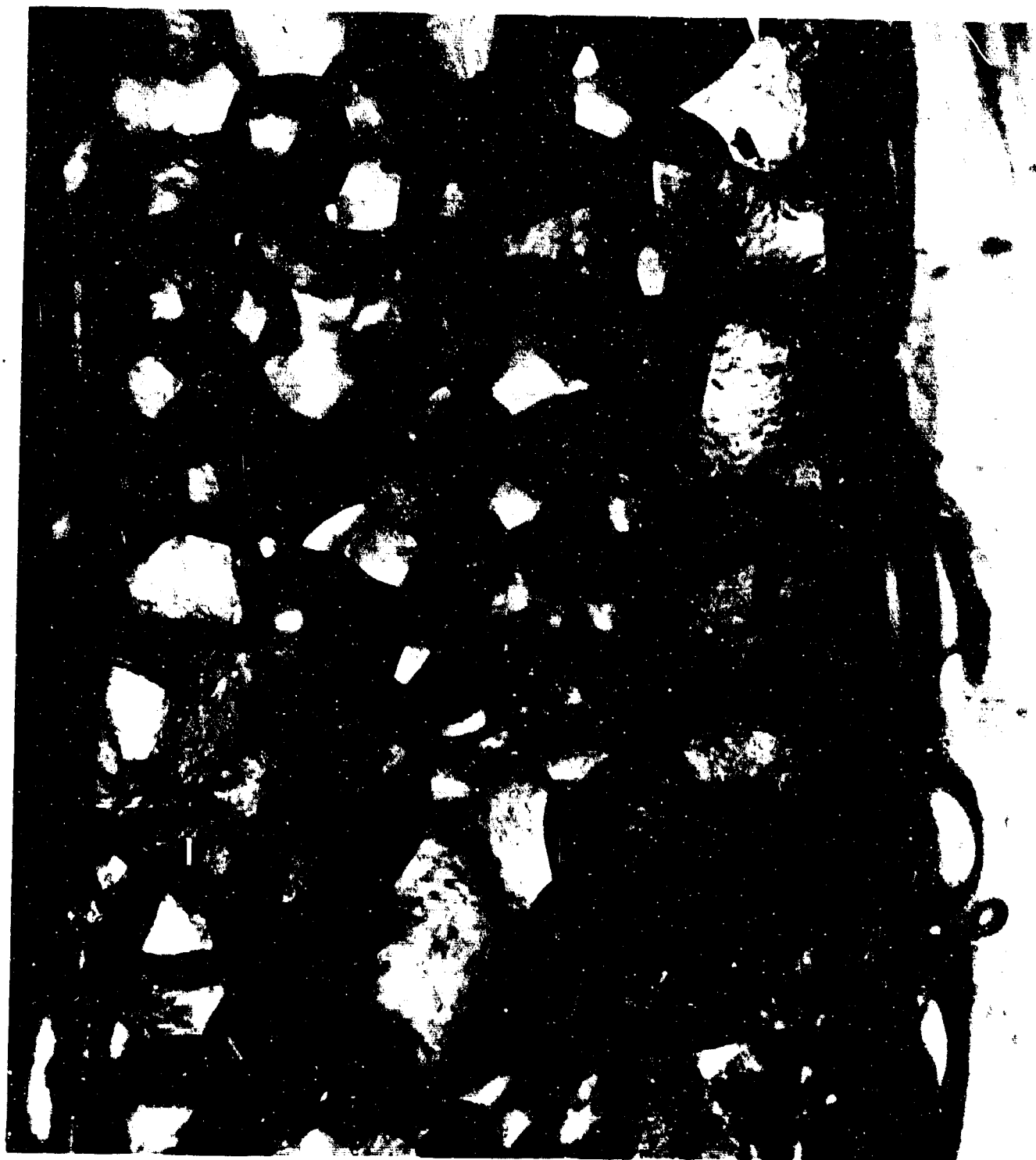
FIGURE 21. ELECTRON MICROGRAPH OF THE TERNARY Al-Zn-Mg ALLOY CATHODICALLY CHARGED IN 5 VOL % ARSENIC-SATURATED H_2SO_4 FOR 35 MINUTES AT 0.02 AMP/CM^2



8750X

J13738

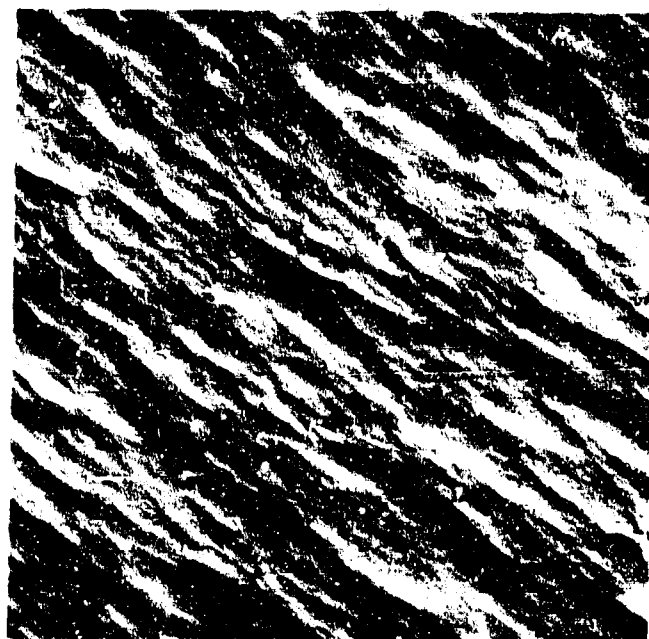
FIGURE 22. ELECTRON MICROGRAPH OF A TERNARY Al-Zn-Mg ALLOY CATHODICALLY CHARGED IN 1N Na_2SO_4 + 0.1 PERCENT SODIUM SILICATE AT $2 \times 10^{-4} \text{ AMP/CM}^2$ FOR 12 HOURS



80X
Compression Edge

L16212
Tension Edge

FIGURE 23 LIGHT MICROGRAPH OF FRACTURE FACE IN THE TERNARY Al-Mg-Zn ALLOY CATHODICALLY CHARGED TO FAILURE



8750X

J13093

a.



8750X

J13082

b.



8750X

J13094

c.

FIGURE 24. ELECTRON MICROGRAPHS OF THE FRACTURE FACE OF THE TERNARY Al-Mg-Zn ALLOY CATHODICALLY CHARGED TO FAILURE

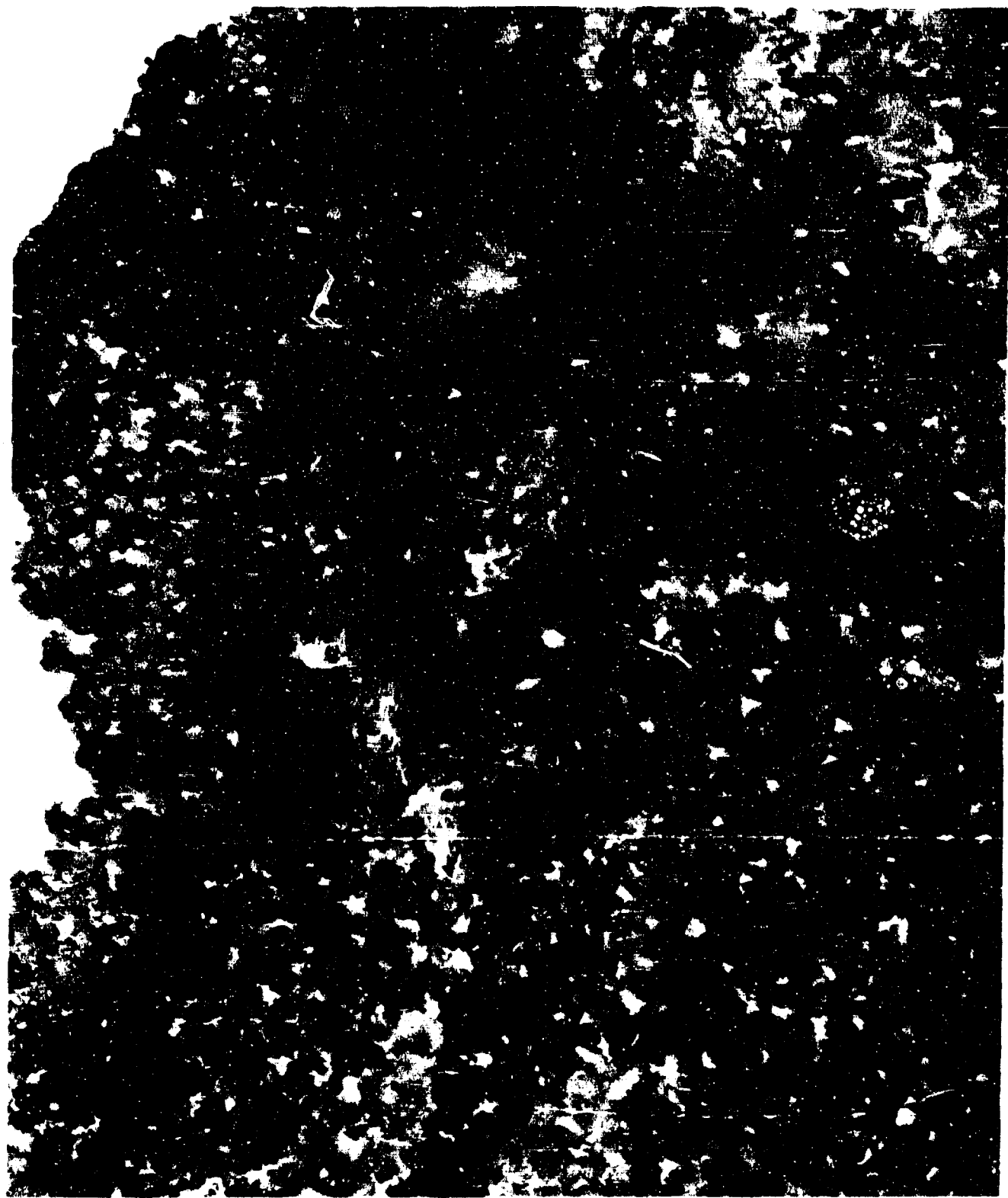
condition. Figure 25 is a transmission electron micrograph of the thin section after cathodic charging for 2 seconds. It can be seen that the grain boundary is not attacked. Also in this particular area, there appears to be a region adjacent to the boundary that differs from the bulk of the grain. Away from the boundary, the grains appear to have been broken into a subgrain structure by hydrogen charging, with pits forming in the subgrain boundary. In addition to this substructure, broad strain contour lines are present in all areas of the hydrogen-charged foil. Prior to charging, these strain contour lines were very narrow, indicating that charging introduces additional strain. It is possible that this strain results from hydrogen entering the subgrain boundaries. Similar broadening of the strain contour lines, and in some areas subgrain boundaries, was observed during corrosion of thin foils, indicating that the cathodic portion of the corrosion reaction may be equivalent to hydrogen charging. Even though the hydrogen may diffuse out during the evacuation of the microscope, the change it has caused in the structure of the metal is apparent. Specimens were also charged in the less severe inhibited Na_2SO_4 solution for times up to 23 hours at high and low current densities and then examined by optical microscopy and by X-ray diffraction. No gross structural or phase changes were detectable except for a pitting-type corrosion when high-current densities were employed. Furthermore, the X-ray diffraction data show no evidence for expansion or strain in the aluminum lattice, indicating that if hydrogen enters the grains there is little or no chemical bonding and the interstitial sites are sufficiently large to accommodate hydrogen atoms. Therefore, the reaction of 7079 alloy with cathodically generated hydrogen may be limited to a solution in the grain-boundary zone.

The hydrogen-ion-metal reaction was investigated by a method (metioscopy) which provides observation of surface characteristics of the aluminum alloy. Electrons emitted from the specimen as a result of bombardment by high-energy hydrogen ions are accelerated by a high voltage, magnified as in an electron microscope, and projected onto a screen or photographic plate, thus providing a magnified image of the specimen surface and reaction thereon. As the hydrogen ion reacts with metals and phases differently, the bombardment results in a variation in electron emission. Also, the surface of the specimen is cathodically etched by the high-energy ions permitting a characterization of the subsurface structure of the material being examined.

For this investigation, a specimen of the ternary Al-Mg-Zn alloy was examined after an electropolish and very light etch. Hydrogen was chosen as the ion gas because of its possible relationship to stress-corrosion cracking in this material. The following experimental conditions were employed:

Cathode voltage: 38 kv
Ion Beam: hydrogen at 19 kv and $10 \mu\text{a}$
Operating pressure: 3×10^{-4} mm Hg

Micrographs of typical structures observed are shown in Figures 26a and 26b. Pits seen in the grain on the right side of these figures are not typical but were chosen as convenient markers for repositioning the specimen so that the same area could be photographed at selected time intervals. After 28 minutes of hydrogen-ion bombardment (cathodic etch) the initially smooth grains begin to exhibit some surface roughness as shown in Figure 26a. A thin zone of slightly higher emission than the matrix is seen along the left side of the grain boundary, while a shallow trough appears to be present along the right side of this grain boundary. Also, precipitate particles are seen in the grain boundary. Further etching (86 minutes) enhances these structural features as seen in Figure 26b. The black zone along the grain boundary, which is enlarged in Figure 26b, results from a shadow cast by the boundary being higher than the adjacent grains. Figure 27 shows a higher magnification view of the grain boundary seen in



45,000X

J13044

FIGURE 25. TRANSMISSION ELECTRON MICROGRAPH OF A THIN SECTION OF THE TERNARY Al-Mg-Zr ALLOY AFTER CATHODIC CHARGING FOR 2 SECONDS



960X

a. 28 Minutes

M-3

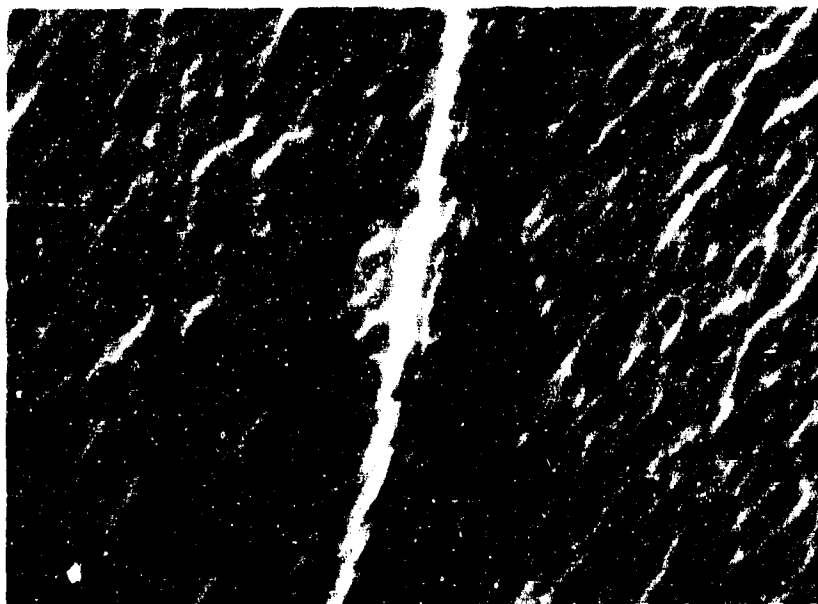


960X

b. 86 Minutes

M-6

FIGURE 26. ELECTRON-EMISSION MICROGRAPHS OF THE TERNARY Al-Mg-Zn ALLOY EXPOSED TO HYDROGEN-ION BOMBARDMENT FOR THE INDICATED TIMES



6400X

M-10

FIGURE 27. ELECTRON-EMISSION MICROGRAPH OF THE TERNARY Al-Mg-Zn ALLOY EXPOSED TO HYDROGEN IONS FOR 165 MINUTES

Figures 26a and 26b. The circle in the center of Figure 27 is the image of the electron-beam aperture, and not a part of the metal structure. Surface undulations are now seen to be in the form of oval-shaped islands and stringers with variable emission, while a high-emission zone at the grain boundary is clearly visible. Black areas to the right of the grain boundary are shadows resulting, as mentioned above, from the grain boundary being in relief with respect to the adjoining grains. Based on the emission efficiencies of aluminum, magnesium, and zinc with hydrogen ions, an area of high emission would be rich in aluminum and/or magnesium and lower in zinc. The significance of these results will be presented in the discussion section.

Microstress Studies

Previous experience has shown that local grain-to-grain variations exist in a nominally uniform stress or strain field. The possibility that such stress concentrations might be significant in the explanation of some aspects of stress corrosion led to the present investigation.

In the present study, the surface strains in the aluminum were determined by bonding thin photoelastic coatings to the surface and photographing the fringe pattern resulting from applied loads. The coatings were then removed and the aluminum specimens were returned for tests in a corrosive environment.

The proposition tested by these procedures is: Does the specimen form corrosion cracks at points of local maximum stress as indicated by the photoelastic tests? If so, this would indicate that (a) scatter in time-to-failure at one nominal stress level, (b) relative insensitivity to nominal stress level, and (c) crack initiation at points not coincident with points of calculated maximum nominal stress might be due in part to these local grain-to-grain stress concentrations.

The alloy used in this test is a high-purity ternary Al-Zn-Mg alloy in the T6 condition. The grains had roughly equal length axes and the average grain diameter was approximately 1/16 inch. Four specimens were prepared. Specimen 1 was tested in a tensile machine giving the proportional limit 49,000 psi, 0.2% offset stress 56,000 psi, and ultimate tensile stress 57,200 psi.

Sheets of photoelastic material 0.010 inch thick were cemented to the top surface of constant-bending-moment Specimens 2, 3, and 4. When viewed in polarized light the relative retardations of the light, as measured by the color of the transmitted light, were proportional to the difference of principal strains in the plane of the specimen surface. These specimens had cross sections that were 0.50 inch wide and 0.22 inch thick and were subjected to constant bending moments by four-point loading, the constant-moment span being 5.5 inches. Photographs of Specimens 2 and 3 were taken at nominal stress levels of 20,000 and 40,000 psi, and of Specimen 4 at 15,000 and 30,000 psi. Final no-load photos were made of all three specimens.

It should be noted that some permanent deformation was induced in Specimens 2 and 4 during these tests. On reviewing the history of these specimens, it was found they were subjected to a straightening procedure, involving temperatures of perhaps 400 F for up to 2 hours. As a result, considerable overaging occurred, lowering the yield stress to between 25,000 to 30,000 psi.

The birefringent coating was removed by mechanically peeling the sheet plastic away from the epoxy cement and degrading this cement by the application of 70 percent concentrated nitric acid. It was also found practical to speed up the epoxy removal by scraping the surface with a wooden stylus.

The order of colors of the photoelastic coatings under polarized light corresponding to increasing principal strain difference was yellow, then red, then blue. Grains with the most highly strained surface planes were those grains with a bluish tone. Points of highest shear strain were noted for each specimen.

The coating was stripped from each specimen and the surface cleaned with nitric acid, followed by a distilled-water wash, and a wipe with benzene. All three specimens were stressed to 40 ksi by four-point loading and exposed to 3.5 percent NaCl by alternate immersion. After 40 hours a stress-corrosion crack had initiated in the specimen which was not overaged. The point of initiation did not correspond to any of the previously noted points of highest shear strain. On the contrary, the point of initiation was between two grains whose grain boundary was very nearly perpendicular to the applied stress. The specimens which were overaged and had exhibited gross localized plastic deformation did not crack within 3 weeks.

DISCUSSION OF RESULTS

The results of the independent phases of study will first be discussed separately, then the consistency of the results will be discussed.

Metallurgical-Variable Studies

This phase of the experimental work revealed several new facts and also confirmed other facts which were not well established. Because this work was done as a statistically designed experiment, these observed facts have statistical significance.

It was shown that for these thin sheet and plate materials, grain shape alone is responsible for the anisotropic stress-corrosion cracking behavior of these aluminum alloys. (It should be noted that other metallurgical variables caused by low cooling rates may contribute to this behavior in thick wrought sections.) Stress-corrosion cracking susceptibility proved to be a function of the stress normal to the grain boundaries rather than the applied stress on a specimen. This is true because there was no significant difference in stress-corrosion cracking behavior between short-transverse and long-transverse specimens when the results were adjusted to common levels of stress normal to the grain boundaries. The ratio of the normal stress to the applied stress was found to be a function of the grain structure and was approximated by assuming the grains to be elongated octahedrons.

It is believed that the techniques used in this study to eliminate the effects of grain structure and stress level are new. It is also believed that this or some similar procedure must be performed before meaningful results can be obtained from the comparison of stress-corrosion-cracking susceptibilities of different alloys.

Table VIII summarizes the metallurgical variable effects found to be statistically significant in this particular experiment. The addition of chromium was expected to be beneficial. However, it was not known if this effect was limited to the long-transverse direction due to its prevention of grain growth or if some other metallurgical effect was present. Because the effect was still significant when the effect of structure and stress level were eliminated, it can be concluded that chromium has an additional beneficial metallurgical effect in these alloys.

There has been some controversy over the beneficial effects of silver in aluminum alloys. This work proves the statistical significance of the effect on stress-corrosion cracking behavior in the particular alloys used. The direct beneficial effect of silver on stress-corrosion-cracking behavior is of the same order of magnitude as that of chromium. However, it is possible that interactions between silver and other metallurgical variables may be more beneficial than chromium interactions with other variables. In this experiment, two significant interaction effects were not separable. These were the interaction between silver and aging treatment and the interaction between chromium and solution heat treatment. The addition of silver and an overaging treatment was beneficial or the addition of chromium and a longer, higher temperature solution heat treatment was beneficial. Based on general principles, both effects are possible. The more severe solution heat treatment should make more of the chromium go into solid solution. This should result in more intragranular precipitate nucleation sites which should be beneficial. On the other hand, silver may delay diffusion of zinc and magnesium to equilibrium precipitate sites when these alloys are overaged, which should also be beneficial.

The addition of copper is detrimental to the stress-corrosion cracking resistance of these particular alloys. The effect is more pronounced for short times than it is for long times. This behavior may indicate that the acceleration of pitting corrosion by copper results in the acceleration of the initiation of stress-corrosion cracks.

A more severe solution heat treatment than normally used is beneficial. The upper limit for the temperature is a function of the melting temperature of the lowest melting phase. The time at temperature is an economic factor rather than metallurgical. This may not be true for all aluminum alloys because of undesirable grain growth which may accompany long solution heat treatments. Also, if relatively insoluble inclusions are present, other metallurgical variables may limit the time for solution heat treatment.

Overaging reduced the susceptibility of these alloys to stress-corrosion cracking. However, this beneficial effect is counteracted by a considerable loss in tensile properties. It may be possible to select aging temperatures and times for alloys containing silver so that the tensile properties are equal to or better than the tensile properties of presently available commercial alloys in the standard T6 condition.

Crack-Kinetics Studies

The relatively inexpensive method developed to study crack propagation gives results comparable with those obtained by the previously used resistance-grid method(14). The observed crack growth rates were continuous, which rules out the electrochemical-mechanical theory as an applicable mechanism. The rates were well within the limits predicted on an electrochemical mechanism. The rate of cracking decreased with a decrease in the original applied stress. The number of cracks initiated

in any one specimen generally increased as the original stress decreased. This may be the result of the stress dependence of the stress-corrosion cracking initiation time. The longer the initiation period for the first crack, the greater the probability that other cracks will initiate.

The bursting of hydrogen bubbles from very small cracks indicates that either extremely severe environmental conditions exist within the crack or that the potential difference between the root of the crack and the walls of the crack is sufficiently large to cause decomposition of water, or both. It is very likely that the pH of the solution within the crack is very low and the oxygen concentration is too low to contribute to the healing of oxide film at the root of the crack.

Electrochemical Studies

The observations of this study are based on a small number of experiments which were conducted while a new technique was being developed. More work is needed to establish with certainty the possibilities these experiments have suggested. The fact that the only failure of a tensile-stressed specimen occurred when both anodic and cathodic charging were present is a strong indication that both reactions must occur on a specimen that stress corrosion cracks. In this particular experiment, it is believed that the cathodically produced hydrogen diffused through the metal along grain boundaries to the anodic side. Hydrogen dissolved in the stressed grain-boundary material apparently decreases the activation energy for the dissolution of the metal by the anodic reaction.

Autoradiographic Studies

These experiments were also few in number and were primarily concerned with the development of a technique. However, the results indicate that hydrogen is present in higher concentrations at grain boundaries of stressed materials that are susceptible to stress-corrosion cracking than in the same material unstressed. Stress apparently preferentially increases the solubility for hydrogen at the grain boundaries.

Precipitate-Phase Studies

Intragranular precipitates are present in alloys containing chromium and are not present in the high-purity ternary Al-Mg-Zn alloy. This is a strong indication that these particular precipitates are rich in chromium. Intergranular precipitates are present in the ternary alloy. The possible combinations of compositions are therefore limited, and it is believed that these precipitates are $MgZn_2$. When copper is present, other compositions are possible and probably are present. However, ϵ -CuZn₄ was ruled out as a probable precipitate.

Fracture-Face Morphology and Surface-Reaction Studies

The morphology of the wall of a stress-corrosion crack adjacent to the crack root is similar in appearance to a polished surface that has been subjected to a severe cathodic charge. This particular appearance does not hold true for the entire crack wall. The wall farther away from the crack tip has an appearance of a surface that has been anodically charged. This behavior indicates that the cathodic current required to produce the anodic current which causes crack growth is supplied by the wall of the crack just adjacent to the crack root. This cell within the crack therefore acts independently of reactions on the surface and on the wall of the crack away from the crack root. There is probably another cell between the latter part of the crack wall and the outside surface which causes anodic dissolution of the crack wall.

Transmission electron micrographs indicate that hydrogen does alter the internal structure of these alloys. However, X-ray diffraction was unable to detect such structural changes. One possibility is that hydrogen is dissolved into interstitial sites and does not cause gross structural changes. Also when under stress, structural changes caused by hydrogen may be confined primarily to grain boundaries. Such changes might be difficult to detect by X-ray diffraction.

The metioscopy technique of direct observation of a surface reacting with high-energy ions revealed that a zone at the grain boundary was low in zinc content in an alloy susceptible to stress-corrosion cracking. This is further proof of the existence of a grain-boundary depleted zone in a susceptible material.

Microstress Studies

Only one of three specimens in this experiment stress-corrosion cracked. This is too small a sample for establishing a definite mechanism. However, the results indicate that stress-corrosion-cracking susceptibility is a function of the stress normal to the grain boundaries rather than the shear strain.

Consistency of the Results of the Independent Studies

The beneficial effects of chromium may be attributed to formation of intragranular rather than intergranular precipitates in these alloys. Silver is known to decrease the tendency for the formation of depleted zones.⁽¹⁸⁾ Its beneficial effect on stress-corrosion cracking behavior may therefore be attributed to this metallurgical characteristic.

Although the results obtained from the electrochemical, autoradiographic, and transmission studies are not conclusive when presented alone, the consistency of the combined results strengthens the belief that cathodically produced hydrogen concentrates at tensile-stressed grain boundaries and reduces the activation energy for the anodic dissolution of the metal.

The results of the single microstress experiment are consistent with the effect of stress determined in the metallurgical variable studies, where 128 specimens were tested.

The consistency of all these independent results suggested a possible mechanism for the initiation of stress-corrosion cracks in these particular alloys.

PROPOSED MECHANISM FOR THE INITIATION OF STRESS CORROSION CRACKS

Stress-corrosion cracking in high-strength aluminum alloys occurs at grain boundaries. There is little doubt that for those alloys susceptible to both intergranular corrosion and stress-corrosion cracking, the failure is by an electrochemical mechanism. However, for those alloys that are not susceptible to intergranular corrosion, the action of stress must produce active grain boundaries before an electrochemical mechanism can initiate cracks. The following proposed mechanism is applicable to the initiation of stress-corrosion cracks in these particular alloys and should also contribute to the initiation of stress-corrosion cracks in alloys susceptible to intergranular corrosion.

Depleted zones in precipitation hardening alloys should be mechanically weaker than the main part of the grains. These zones are expected to plastically deform at relatively low stresses; however, their extremely small volume restricts the total amount of flow that may occur. Thus, small notches should form at grain boundaries. The material at the root of a notch is in a triaxial state of stress and has a higher hydrostatic stress component than does the grain which is subjected only to a uniaxial tension stress. If we assume that the change in notch geometry in the mechanically weak zones is such that the flow stress is maintained but not exceeded, the hydrostatic-stress component will equal the applied stress less two-thirds of the flow stress for the weak material. The hydrostatic stress component on the grains is one third of the applied stress.

The difference in the hydrostatic stress components between the grains and grain boundaries will cause a small difference in strain energy which will be relieved by absorbing an interstitial such as hydrogen. When equilibrium is reached, more hydrogen will be in solution at grain boundaries than within the grains in order to balance out the effect of the difference in the hydrostatic stress components and make the total free-energy change be zero. An interstitial solute such as hydrogen should reduce the activation energy for the dissolution of the metal. This does not alter the equilibrium potential but increases the exchange current for the equilibrium between metal and metal ions, which in turn shifts the position of the anodic potential-current curve.

It is reasonable to assume that the displacement between the anodic curve on the grain boundaries and the anodic curve on the grains is a function of the ratio of the hydrostatic stress components. This ratio is

$$\frac{3\sigma - 2K}{\sigma} = \text{hydrostatic-stress component ratio,} \quad (2)$$

where σ is the applied stress and K is the flow stress of the weak zone material. For any given potential, the ratio of the anodic current at the grain boundaries (i_{gb}) to the anodic current on the grains (i_g) is

$$\frac{i_{gb}}{i_g} = f \left(\frac{3\sigma - 2K}{\sigma} \right) \quad (3)$$

This ratio applies when equilibrium is reached; however, the rate at which equilibrium is approached is controlled by the diffusion of hydrogen into the grains and grain boundaries. Because of the extremely small area of the grain boundaries, most of the hydrogen in the grain boundaries will arrive by diffusion through the grains. An exact solution to this unsteady-state-diffusion problem may be impossible. However, a function often involved in unsteady-state-diffusion problems may be used as an approximation. This relationship is

$$\frac{c}{c_0} = e^{-\frac{L^2}{\sigma D t}}, \quad (4)$$

where c and c_0 are instantaneous and equilibrium concentrations of hydrogen at the grain boundary depleted zones respectively, L is the average distance of diffusion through the grains, D is a diffusion constant, σ is the applied stress, and t is the time. This approximate solution meets the boundary condition

$$\begin{aligned} c &= 0 \text{ at } t = 0 & c &= c_0 \text{ at } t = \infty \\ \frac{\partial c}{\partial t} &= 0 \text{ as } t \rightarrow 0 & \frac{\partial c}{\partial t} &= 0 \text{ at } t = \infty \end{aligned} \quad (5)$$

The right side of Equation (4) may be used as a time-dependent correction factor for Equation (3). We now have

$$\frac{i_{gb}}{i_g} = f\left(\frac{3\sigma - 2K}{\sigma}\right) \cdot e^{-\frac{L^2}{\sigma D t}}. \quad (6)$$

The difference in anodic current density at the grain boundaries and at the grains is a measure of the tendency for localized corrosion such as stress-corrosion cracking. This difference is

$$(i_{gb} - i_g) = i_g \left[f\left(\frac{3\sigma - 2K}{\sigma}\right) \cdot e^{-\frac{L^2}{\sigma D t}} - 1 \right]. \quad (7)$$

The transition from the initiation to the propagation stage of stress-corrosion cracking is a continuous process that is a function of the change in the crack geometry and the environment within the crack. Equation (7) will not be applicable to the propagation stage. Thus, we may arbitrarily define the initiation stage as that portion of the process to which Equation (7) is applicable, limited by a particular crack depth which is equivalent to some constant number of coulombs per unit area. The exponential term in Equation (7) can be approximated by the first two terms in the equivalent infinite series. The total amount of current flow to initiate the crack is

$$Q = \int_{t_0}^t (i_{gb} - i_g) dt = i_g \left\{ \left[f\left(\frac{3\sigma - 2K}{\sigma}\right) \right] \left[(t - t_0) - \frac{L^2}{\sigma D} \ln \frac{t}{t_0} \right] \right\} - i_g(t - t_0), \quad (8)$$

where t_0 is some minimum time below which a purely mechanical failure mechanism is applicable. When K is small with respect to σ and t is not much greater than t_0 , the stress time for crack initiation relationship simplifies to

$$\sigma = a - b \ln t, \quad (9)$$

where a and b are constants. However, when σ is small and t is large, the other terms cannot be neglected and a complex relationship results which predicts that the stress-corrosion-cracking endurance will approach infinity as the stress is lowered to the flow stress of the weak depleted zones. The flow stress K represents the stress below which no stress-corrosion cracking will occur.

Once the crack is initiated, the conditions become much more favorable for an electrochemical reaction. The stress on the walls of the crack become negligible, which results in an increased potential difference between the walls of the crack and the crack root. Precipitation of corrosion products at the mouth of the crack leaves the solution within the crack more acidic. The lowering of pH provides more hydrogen ions for the rate-controlling cathodic reaction and increases the solubility of aluminum in aqueous solution. The reaction within the crack, therefore, becomes autocatalytic.

This theory appears to be consistent with stress-corrosion-cracking behavior. The following predictions based on this theory agree with facts observed during the course of this research:

- (1) Metallurgical variables which decrease the probability of weak depleted zones in high-strength aluminum alloys should increase the resistance to stress-corrosion cracking.
- (2) Shear stresses at weak grain boundaries will cause slip rather than increase the hydrostatic stress component; therefore, stress-corrosion cracking susceptibility is a function of the stress normal to the grain boundaries rather than the stress applied to the specimen.
- (3) Because hydrogen must be present to make the grain boundaries more active and the crack progresses by anodic dissolution of the metal, both anodic and cathodic reactions must be present on the metal.
- (4) Crack-propagation kinetics should be continuous rather than discontinuous.
- (5) At equilibrium conditions (for a high-strength aluminum alloy susceptible to stress-corrosion cracking stressed in tension in a corrosive environment) there should be a higher concentration of hydrogen at the grain boundaries than in the grains.

CONCLUSIONS

Existing theories for the mechanism for stress-corrosion cracking in our opinion do not satisfactorily explain the observed behavior of high-strength aluminum alloys. The only fairly consistent theory prior to this investigation was the electrochemical - mechanical theory. The crack-kinetics studies did not reveal any fast fracture steps which would be necessary for such a mechanism. Also, the observed continuous crack rates were well within the limits predicted by an electrochemical mechanism.

Intergranular stress-corrosion cracking in these 7039 and 7079 type alloys is a function of the stress normal to the grain boundaries rather than the applied stress. This fact must be considered if meaningful comparisons of stress-corrosion cracking susceptibilities of different alloys are to be made. An elongated octahedral structure proved to be a good approximation of grain shape. This approximation made it possible to eliminate the effects of stress and grain shape so that alloys of different composition could be compared.

The addition of chromium, the addition of silver, severe solution heat treatment, overaging, and the combination of silver and overaging or the combination of chromium and severe solution heat treatment were all beneficial to the stress-corrosion-cracking resistance of these alloys. The addition of copper was detrimental.

The combined results of the electrochemical, autoradiographic, electron-transmission, and replica studies are consistent with the proposed mechanism for the initiation of stress-corrosion cracks. This mechanism involves the absorption of cathodically produced hydrogen into strained mechanically weak grain boundaries. The hydrogen acts to reduce the activation energy for the anodic dissolution of the metal and thus accelerates the localized corrosion at the grain boundaries perpendicular to applied tensile stresses.

REFERENCES

- (1) E. H. Dix, Jr., "Acceleration of the Rate of Corrosion by High Constant Stresses", Trans. Inst. of Metals, AIME, 137, Techn. Publ. No 1204, 1940.
- (2) J. G. Hines, "Propagation of Stress-Corrosion Cracks in Metals", Corrosion Science, 1, 21-48 (August 1961).
- (3) D. O. Sprowls and R. H. Brown, "What Every Engineer Should Know About Stress Corrosion of Aluminum", Metals Progress, 81, 79-85 (April 1962); 77 (May 1962).
- (4) F. A. Champion, "The Interaction of Static Stress and Corrosion With Aluminum Alloys", Journal of the Institute of Metals, 83, 385-392 (1955).
- (5) H. L. Logan, "Film-Rupture Mechanism of Stress Corrosion", J. of Res. of Nat. Bur. Std., 48, 99-105 (February 1952).
- (6) P. R. Swann, "Stress-Corrosion Failure", Scientific American, 214, 73-81 (February 1966).
- (7) E. N. Pugh and W. R. D. Jones, "The Mechanism of Stress-Corrosion in a High-Purity Aluminum-Zinc-Magnesium Alloy", Metallurgia, 63, 3 (January 1961).
- (8) G. E. Dieter, Jr., Mechanical Metallurgy, McGraw-Hill Book Co., Inc., New York, N. Y. (1961), pp 194-198.
- (9) E. A. G. Liddiard, "The Mechanical Influence of Corrosion on Metals - Parts 1 and 2", Corrosion Technology, 10 (3), 65-67 (March 1963); (4), 95-97 (April 1963).

- (10) T. N. Rhodin, Ed., Physical Metallurgy of Stress Corrosion Fractures, Interscience Publishers, New York, N. Y. (1959), pp 29-46, 79-98, 341-372.
- (11) D. van Rooyen, "Stress Corrosion Cracking", Tech. Report No. 1, Contract No. NR-2868(00), NR 036-044, 2-2-26-59, Office of Naval Research (November 10, 1959).
- (12) R. N. Parkins, Lecture on Stress-Corrosion Cracking, The Ohio State University, (March 21, 1966).
- (13) E. G. Coleman, D. Weinstein, and W. Rostoker, "On the Surface Energy Mechanism for Stress Corrosion Cracking", Acta Metallurgica, 9, 491 (May 1961).
- (14) F. H. Haynie, D. A. Vaughn, W. K. Boyd, and P. D. Frost, "An Investigation of the Nature of Stress-Corrosion Cracking in Aluminum Alloys", Annual Summary Report, AFML-TR-65-258, Air Force Materials Laboratory, Wright-Patterson Air Force Base, Ohio (July 1965).
- (15) F. F. Booth and G. E. G. Tucker, "Statistical Distribution of Endurance in Electrochemical Stress-Corrosion Tests", Corrosion, 21 (5), 73 (May 1965).
- (16) F. S. Prestley, "Effect of Specimen Orientation on Resistance to Stress-Corrosion Cracking of Aluminum Alloys - A Mathematical Model", Reynolds Metals Co., Submitted for publication to ASTM, oral communication.
- (17) W. Gruhl, "Der Einfluss der Korrosionsbedingungen auf das Spannungsresskorrosionsverhalten von AlZnMg", Metallwissenschaft und Technik, 17, 197 (March 1963).
- (18) J. J. Polmear, "Studies on High-Strength Aluminum Alloys in Australia", Metal Progress, 82, 82 (January 1962).

A-1

APPENDIX A

The two-level factorial design experiment is an excellent method for determining which variables have an effect on the outcome. The significance of each effect can be determined by analysis of variance.

As many variables as possible that may be expected to have an effect on the outcome should be included in the original experiment. In order to simplify the following example, only three variables will be used.

Suppose that one alloy contains silver and another does not, and in addition, that the effects of cold working and overaging are to be studied. The following nomenclature is then assigned:

A+ Alloy with silver

B+ With cold work

C+ With overage

A- Alloy without silver

B- Without cold work

C- Without overage

The factorial design is:

		A+		A-	
		B+	B-	B+	B-
C+	C+				
	C-				

This experiment requires eight entirely different sets of conditions. In order to determine the within-sample error more accurately, it is wise to replicate each condition. It is thus necessary to perform a minimum of 16 separate tests. In this particular example, the outcome is the log of the endurance of each stress-corrosion specimen.

		A+		A-	
		B+	B-	B+	B-
C+	C+	1.86	2.54	2.01	3.02
	C-	1.95	2.43	2.32	2.89
C-	C+	1.65	2.32	1.98	2.56
	C-	1.73	2.25	1.87	2.60

A-2

Each response can be identified by its location. For example, y_{A+B+C+} has two responses, which are 1.86 and 1.95. They can be further subscripted as $y_{A+B+C+1}$ and $y_{A+B+C+2}$. The error sum of squares for the experiment is:

$$\sum_{i_1 j_1 k_1}^{A+B+C+} \left(\sum_{\ell=1}^2 y_{(i)j k \ell}^2 - \left[\frac{1}{2} \sum_{\ell=1}^2 y_{(i)j k} \right]^2 \right)$$

Each pair of responses must be squared, then added, and also added then squared. For example, the responses for $A+B+C+$ would be treated in the following manner:

$$(1.86)^2 + (1.95)^2 - 1/2 [1.86 + 1.95]^2 = .010$$

Each of these figures is then summed, to give the error sum of squares, which in this example is 0.14. The error degree of freedom is $(2-1) \times 8 = 8$. The 2 is the number of times the response is replicated, the 1 is for each different condition, and the 8 is the number of conditions.

In studying the effects of variables it is mathematically easier to work with differences between levels rather than with means at each level. The difference is referred to as a contrast.

$$\hat{A} = \frac{1}{N} [\sum y_+ - \sum y_-]$$

where

\hat{A} = the contrast or effect of silver

N = the number of tests, which is 16

y_+ = any response in the $A+$ columns

y_- = any response in the $A-$ columns.

\hat{B} and \hat{C} are calculated in a similar manner. The interactions \hat{AB} , \hat{AC} , \hat{BC} , and \hat{ABC} use the same procedure, except the signs for the responses are determined by products of the signs for the variables. For example, $(A+)(B+)$ is $\hat{AB}(+)$ and $(A+)(B+)(C-)$ is $\hat{ABC}-$. For \hat{AB} , $A+B+$ is $(+)$, $A+B-$ is $(-)$, $A-B+$ is $(-)$, and $A-B-$ is $(+)$. The absolute value of each response remains the same. Each effect or contrast has $(2-1)$ degrees of freedom. The 2 is for the replication, and the 1 is for each condition.

Each contrast is squared and multiplied by the number of tests (16) to obtain the sum of squares. Table A-1 shows the values as they are used in analysis of variance.

F is the ratio of the sum of squares of the effect to the error sum of squares. An F distribution table shows that for 1 degree of freedom for the greater sum of squares and 8 degrees of freedom for the lesser sum of squares, the 5 percent and 1 percent

levels of F are 5.32 and 11.25, respectively. Thus, in this example, there is less than 1 percent probability that the B effect is caused by random error. On the other hand, the remainder of the effects are not significant.

TABLE A-1. ANALYSIS OF VARIANCE

Effect	Contrast	Sum of Squares	Degrees of Freedom	F
\hat{A}	-0.1568	0.393	1	2.81
\hat{B}	-0.3275	1.716	1	12.25
\hat{C}	+0.1287	0.265	1	1.89
\hat{AB}	+0.0337	0.018	1	0.129
\hat{AC}	-0.025	0.010	1	0.071
\hat{BC}	-0.013	0.0028	1	0.020
\hat{ABC}	+0.0188	0.0056	1	0.040
Error		0.14	8	

If this were a true problem, it would show that materials without cold work were not as susceptible to stress-corrosion cracking as materials with cold work. The addition of silver and overaging had no significant effect. Note that this is a hypothetical example.

Each time an additional variable is to be studied, twice as many experiments must be performed to complete the two-level factorial design. When many variables are involved, the number of experiments becomes prohibitive.

Fractional replication can be used to reduce the amount of testing. When this is done, the amount of information that can be obtained from the experiment is also reduced.

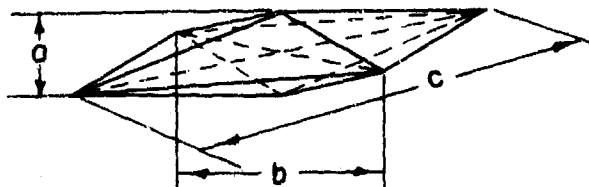
The example of the factorial design with three variables will be used. However, the negative side of the ABC contrast will not be tested for.

	A+		A-	
	B+	B-	B+	B-
C+	1.86			3.02
	1.95			2.89
C-		2.32	1.98	
		2.25	1.87	

With the previous method for analysis of variance it is found that ABC cannot be obtained, because the negative values are missing, and that contrasts $A = BC$, $B = AC$, and $C = AB$. In this particular example, an assumption that all the interaction effects are unimportant is correct and it is possible to arrive at the same conclusions that were obtained from the full factorial design experiment. In some cases, it may be that the interaction effects are much greater than the effects of the main variables, in which case an assumption would lead to drastically wrong conclusions. It is wise to have some idea about the effect of interactions before fractional replication is used.

APPENDIX B

Assume an elongated octahedral crystal.



Assume that stress is applied parallel to a and calculate the fraction of stress acting perpendicular to the faces. Resolve forces

$$\frac{F'}{F} = \frac{b/2}{\sqrt{\frac{a^2}{4} + \frac{b^2}{4}}} = \frac{b}{\sqrt{a^2 + b^2}}$$

$$\frac{x}{b/2} = \frac{a/2}{\sqrt{\frac{a^2}{4} + \frac{b^2}{4}}} \quad x = \frac{ab}{2\sqrt{a^2 + b^2}}$$

$$\frac{F''}{F'} = \frac{c/2}{\sqrt{x^2 + \frac{c^2}{4}}} = \frac{C}{2\sqrt{\frac{a^2b^2}{4(a^2 + b^2)} + \frac{c^2}{4}}} = \frac{C\sqrt{a^2 + b^2}}{\sqrt{a^2b^2 + c^2(a^2 + b^2)}}$$

$$\frac{F'''}{F} = \frac{bc}{\sqrt{a^2b^2 + c^2(a^2 + b^2)}}$$

The dimensions a, b, and c represent relative grain dimensions, with the a-dimension parallel to the applied stress. Stress σ is the force, F, acting on a unit area, A, of cross section.

Therefore:

$$\sigma = \frac{F}{A}, \quad \frac{\sigma_{\text{normal}}}{\sigma_{\text{applied}}} = \frac{F''A}{FA''}$$

A similar calculation shows that

$$\frac{A}{A''} = \frac{bc}{\sqrt{a^2b^2 + c^2(a^2 + b^2)}}$$

Thus:

$$\frac{\sigma_{\text{normal}}}{\sigma_{\text{applied}}} = \frac{b^2 c^2}{a^2 b^2 + c^2 (a^2 + b^2)}$$

UNCLASSIFIED

Security Classification

DOCUMENT CONTROL DATA - R&D		
(Security classification of title, body of abstract and indexing annotation must be entered when the overall report is classified)		
1. ORIGINATING ACTIVITY (Corporate author)		2a. REPORT SECURITY CLASSIFICATION
Battelle Memorial Institute Columbus, Ohio		UNCLASSIFIED
		2b. GROUP
		N/A
3. REPORT TITLE		
A FUNDAMENTAL INVESTIGATION OF THE NATURE OF STRESS-CORROSION CRACKING IN ALUMINUM ALLOYS		
4. DESCRIPTIVE NOTES (Type of report and inclusive dates)		
Final report - June 1965 to May 1966		
5. AUTHOR(S) (Last name, first name, initial)		
Haynie, F. H., Vaughan, D. A., Phalen, D. I., Boyd, W. K., and Frost, P. D.		
6. REPORT DATE	7a. TOTAL NO. OF PAGES	7b. NO. OF REFS
January 1967	68	18
8a. CONTRACT OR GRANT NO. AF 33(615)-1710	9a. ORIGINATOR'S REPORT NUMBER(S)	
b. PROJECT NO. 7351	AFML-TR-66-267	
c. TASK NO. 735106	9b. OTHER REPORT NO(S) (Any other numbers that may be assigned this report)	
d.		
10. AVAILABILITY/LIMITATION NOTICES This document is subject to special export controls and each transmittal to foreign governments or foreign nationals may be made only with prior approval of the Metals and Ceramics Division (MAM), Air Force Materials Laboratory, Wright-Patterson AFB, Ohio 45433.		
11. SUPPLEMENTARY NOTES		12. SPONSORING MILITARY ACTIVITY
		Metals and Ceramics Division Air Force Materials Laboratory, RTD Wright-Patterson AFB, Ohio
<p>Several experimental techniques are used to study the mechanisms of stress-corrosion cracking in high purity aluminum alloys. The effect of metallurgical variables such as alloying elements (Cr, Ag, Cu) and heat treatments on a 4.2Zn-3.3Mg aluminum alloy are determined. Techniques used in this study include electrode polarization, autoradiographic studies, microstress studies, electron microscopy (replica and transmission), metioscopy, and standard stress-corrosion testing methods.</p> <p>As a result of these studies, an electrochemical theory for the mechanism of stress-corrosion cracking which involves the strain induced absorption of hydrogen is found to be consistent with the observations.</p>		

DD FORM 1473

UNCLASSIFIED

Security Classification

UNCLASSIFIED

Security Classification

14 KEY WORDS	LINK A		LINK B		LINK C	
	ROLE	WT	ROLE	WT	ROLE	WT
Stress-corrosion cracking High purity 703P - 7079 Aluminum alloys Effect of hydrogen dislocation networks grain - boundary voids NaCl solution						

INSTRUCTIONS

1. **ORIGINATING ACTIVITY:** Enter the name and address of the contractor, subcontractor, grantee, Department of Defense activity or other organization (*corporate author*) issuing the report.

2a. **REPORT SECURITY CLASSIFICATION:** Enter the overall security classification of the report. Indicate whether "Restricted Data" is included. Marking is to be in accordance with appropriate security regulations.

2b. **GROUP:** Automatic downgrading is specified in DoD Directive 5200.10 and Armed Forces Industrial Manual. Enter the group number. Also, when applicable, show that optional markings have been used for Group 3 and Group 4 as authorized.

3. **REPORT TITLE:** Enter the complete report title in all capital letters. Titles in all cases should be unclassified. If a meaningful title cannot be selected without classification, show title classification in all capitals in parenthesis immediately following the title.

4. **DESCRIPTIVE NOTES:** If appropriate, enter the type of report, e.g., interim, progress, summary, annual, or final. Give the inclusive dates when a specific reporting period is covered.

5. **AUTHOR(S):** Enter the name(s) of author(s) as shown on or in the report. Enter last name, first name, middle initial. If military, show rank and branch of service. The name of the principal author is an absolute minimum requirement.

6. **REPORT DATE:** Enter the date of the report as day, month, year, or month, year. If more than one date appears on the report, use date of publication.

7a. **TOTAL NUMBER OF PAGES:** The total page count should follow normal pagination procedures, i.e., enter the number of pages containing information.

7b. **NUMBER OF REFERENCES:** Enter the total number of references cited in the report.

8a. **CONTRACT OR GRANT NUMBER:** If appropriate, enter the applicable number of the contract or grant under which the report was written.

8b, 8c, & 8d. **PROJECT NUMBER:** Enter the appropriate military department identification, such as project number, subproject number, system numbers, task number, etc.

9a. **ORIGINATOR'S REPORT NUMBER(S):** Enter the official report number by which the document will be identified and controlled by the originating activity. This number must be unique to this report.

9b. **OTHER REPORT NUMBER(S):** If the report has been assigned any other report numbers (*either by the originator or by the sponsor*), also enter this number(s).

10. **AVAILABILITY/LIMITATION NOTICES:** Enter any limitations on further dissemination of the report, other than those

imposed by security classification, using standard statements such as:

- (1) "Qualified requesters may obtain copies of this report from DDC."
- (2) "Foreign announcement and dissemination of this report by DDC is not authorized."
- (3) "U. S. Government agencies may obtain copies of this report directly from DDC. Other qualified DDC users shall request through _____."
- (4) "U. S. military agencies may obtain copies of this report directly from DDC. Other qualified users shall request through _____."
- (5) "All distribution of this report is controlled. Qualified DDC users shall request through _____."

If the report has been furnished to the Office of Technical Services, Department of Commerce, for sale to the public, indicate this fact and enter the price, if known.

11. **SUPPLEMENTARY NOTES:** Use for additional explanatory notes.

12. **SPONSORING MILITARY ACTIVITY:** Enter the name of the departmental project office or laboratory sponsoring (*paying for*) the research and development. Include address.

13. **ABSTRACT:** Enter an abstract giving a brief and factual summary of the document indicative of the report, even though it may also appear elsewhere in the body of the technical report. If additional space is required, a continuation sheet shall be attached.

It is highly desirable that the abstract of classified reports be unclassified. Each paragraph of the abstract shall end with an indication of the military security classification of the information in the paragraph, represented as (TS), (S), (C), or (U).

There is no limitation on the length of the abstract. However, the suggested length is from 150 to 225 words.

14. **KEY WORDS:** Key words are technically meaningful terms or short phrases that characterize a report and may be used as index entries for cataloging the report. Key words must be selected so that no security classification is required. Identifiers, such as equipment model designation, trade name, military project code name, geographic location, may be used as key words but will be followed by an indication of technical context. The assignment of links, rules, and weights is optional.

UNCLASSIFIED

Security Classification